Diminished force production and mitochondrial respiratory deficits are strain-dependent myopathies of subacute limb ischemia

Cameron A. Schmidt, BS,[a,b] Terence E. Ryan, PhD,[a,b] Chien-Te Lin, PhD,[a,b] Melissa M. R. Inigo, BS, MS,[a,b] Tom D. Green, BS,[a,b] Jeffrey J. Brault, PhD,[b,c] Espen E. Spangenburg, PhD,[a,b] and Joseph M. McClung, PhD,[a,b] *Greenville, NC*

Objective: **Reduced skeletal muscle mitochondrial function might be a contributing mechanism to the myopathy and activity based limitations that typically plague patients with peripheral arterial disease (PAD). We hypothesized that mitochondrial dysfunction, myofiber atrophy, and muscle contractile deficits are inherently determined by the genetic background of regenerating ischemic mouse skeletal muscle, similar to how patient genetics affect the distribution of disease severity with clinical PAD.**

Methods: **Genetically ischemia protected (C57BL/6) and susceptible (BALB/c) mice underwent either unilateral subacute hind limb ischemia (SLI) or myotoxic injury (cardiotoxin) for 28 days. Limbs were monitored for blood flow and tissue oxygen saturation and tissue was collected for the assessment of histology, muscle contractile force, gene expression, mitochondrial content, and respiratory function.**

Results: **Despite similar tissue O_2 saturation and mitochondrial content between strains, BALB/c mice suffered persistent ischemic myofiber atrophy (55.3% of C57BL/6) and muscle contractile deficits (approximately 25% of C57BL/6 across multiple stimulation frequencies). SLI also reduced BALB/c mitochondrial respiratory capacity, assessed in either isolated mitochondria (58.3% of C57BL/6 at SLI on day (d)7, 59.1% of C57BL/6 at SLI d28 across multiple conditions) or permeabilized myofibers (38.9% of C57BL/6 at SLI d7; 76.2% of C57BL/6 at SLI d28 across multiple conditions). SLI also resulted in decreased calcium retention capacity (56.0% of C57BL/6) in BALB/c mitochondria. Nonischemic cardiotoxin injury revealed similar recovery of myofiber area, contractile force, mitochondrial respiratory capacity, and calcium retention between strains.**

Conclusions: **Ischemia-susceptible BALB/c mice suffered persistent muscle atrophy, impaired muscle function, and mitochondrial respiratory deficits during SLI. Interestingly, parental strain susceptibility to myopathy appears specific to regenerative insults including an ischemic component. Our findings indicate that the functional deficits that plague PAD patients could include mitochondrial respiratory deficits genetically inherent to the regenerating muscle myofibers. (J Vasc Surg 2017;65:1504-14.)**

Clinical Relevance: **Skeletal muscle morphology and function are key predictors of clinical manifestation and outcomes in peripheral arterial disease. Our findings show that genetic background is a critical determinant of muscle functional deficits and mitochondrial respiration. Because of the range of peripheral arterial disease manifestations, BALB/c mice provide a useful model for studying the role of muscle and mitochondrial respiratory functional abnormalities in determining morbidity and mortality outcomes in genetically susceptible patients. Novel therapies that directly target the muscle tissue response to limb ischemia could be used alone or in conjunction with current revascularization therapies to reduce morbidity and mortality outcomes in claudicants or patients with critical limb ischemia.**

From the Department of Physiology,[a] Diabetes and Obesity Institute, Brody School of Medicine,[b] and Department of Kinesiology,[c] East Carolina University.

This work was supported in part by an East Carolina University East-West Collaborative Research Award to J.M.M. and J.J.B. E.E.S. was supported by NIH/NIAMS R01AR066660. J.M.M. was supported by NIH/NHLBI R00HL103797 and R01HL125695.

Author conflict of interest: none.

Additional material for this article may be found online at www.jvascsurg.org.

Correspondence: Joseph M. McClung, PhD, Diabetes and Obesity Institute, East Carolina Heart Institute, Brody School of Medicine at East Carolina University, Office #4109, Mail Stop 743, 115 Heart Dr, Greenville, NC 27834-4354 (e-mail: mcclungj@ecu.edu).

The editors and reviewers of this article have no relevant financial relationships to disclose per the JVS policy that requires reviewers to decline review of any manuscript for which they may have a conflict of interest.

0741-5214

http://dx.doi.org/10.1016/j.jvs.2016.04.041

The recent identification of differences in the clinical course of intermittent claudication (pain with exertion that is relieved with rest) and critical limb ischemia (CLI, pain at rest with or without tissue necrosis or gangrene) raise the intriguing possibility that these represent genetically determined and distinct phenotypic manifestations of peripheral arterial disease (PAD).[1-7] Preclinically, different inbred mouse strains have dramatically different responses to a murine model of limb ischemia, analogous to the range of responses seen in human patients. For example, BALB/c mice show substantial muscle necrosis after subacute and acute models of ischemia similar to the myopathy observed in patients with CLI, whereas C57BL/6 mice recover rapidly from ischemia without substantial tissue loss or myopathy.[2,3,8,9] Genetic haplotype analysis in these mice identified a quantitative trait locus

associated with tissue necrosis that contained 37 genes with no known role in vascular biology.[3] The findings from these studies implies that genetic susceptibility to limb ischemia might be a key factor in the pathology of PAD/CLI. The possibility of genetic regulation of ischemic limb (L) pathology is further highlighted by the underwhelming results of angiogenic/neovascularization clinical trials[10] in PAD patients.

Patients with PAD, in addition to vascular defects, have altered muscle metabolism, mitochondrial respiration, expression of mitochondrial enzymes, increased oxidative stress, and somatic mutations in mitochondrial genes.[11-17] This implies that reduced skeletal muscle mitochondrial function might be a contributing mechanism to the myopathy and activity based limitations that typically plague these patients. We hypothesized that mitochondrial dysfunction, myofiber atrophy, and contractile deficits are inherently determined by the genetic background of the murine regenerating ischemic skeletal muscle. Our findings indicated that myopathy associated with subacute ischemia uniquely involves mitochondrial functional abnormalities that parallel deficits in muscle function and regeneration. Although the functional deficits that plague PAD patients might initially be caused by occlusive obstruction of blood flow to the limb, the inability to recover muscle mass and function might involve analogous mitochondrial respiratory deficits genetically inherent to the muscle myofibers.

METHODS

Detailed information is shown in the Appendix (online only).

Animals. Experiments were conducted on adult (aged 12-16 week) C57BL/6J (n = 33) or BALB/cJ (n = 36) mice. All work was approved by the Institutional Review Committee of East Carolina University and complied with the *Guide for the Care and Use of Laboratory Animals.*[18] Subacute ischemia was performed as previously described.[9] The cardiotoxin (CTX) model of mouse muscle regeneration was performed as previously described[19] using intramuscular injections of *Naja nigricollis* venom.

Assessment of limb perfusion and O_2 saturation of tissue. Limb blood flow was measured using laser Doppler perfusion imaging (LDPI) as previously described.[9] Tissue oxygen saturation (SO_2) was assessed using a moorVMS-OXY white light spectrometer with a CPT-300 optical probe (Moor Instruments, Devon, United Kingdom).

Immunofluorescence and histological analysis. Skeletal muscle morphology, lipid and collagen deposition, vessel density, and muscle myofiber phenotype were assessed using standard light microscopy and immunofluorescence (IF). IF and microscopy muscle regeneration was assessed using magnification ×40 tiled hematoxylin and eosin (H&E) images using an Aperio CS2 digital slide analyzer (Leica Biosystems, Buffalo Grove, Ill). Lipid droplet content was assessed using Oil Red-O counterstained in Mayer hematoxylin, as well as IF for dystrophin and boron-dipyrromethene (BODIPY) 493/503 (Thermo Fisher Scientific, Waltham, Mass). Collagen deposition was visualized using staining in Weigert hematoxylin solution and picrosirius red (PR). Vascular density was assessed using IF as previously described[8,9] and is presented as the mean CD31-positive ($CD31^+$) area per magnified ×20 field of view. Muscle fiber typing was performed as previously described[20] using IF and presented as a proportion of total myofibers of each fiber type (myosin heavy chain [MHC] type IIa, MyHC type IIb, or MyHC type IIx).

Immunoblot analysis. Western blotting was performed using standard methods. Blots were visualized with chemiluminescence using standard film procedures.

Preparation of isolated skeletal muscle mitochondria for respirometry. Skeletal muscle mitochondria were isolated from the gastrocnemius, plantaris, and soleus muscles as described.[21] High-resolution O_2 consumption measurements were conducted using the OROBOROS O2K Oxygraph (Oroboros Instruments Corp, Innsbruck, Austria). The rate of respiration was expressed as pmol/s/mg mitochondrial protein.

Preparation of permeabilized muscle fibers for myofiber respiration. A portion of the red gastrocnemius muscle was removed and fiber bundles were separated along their longitudinal axis as previously described.[22] The rate of respiration was normalized to the myofiber dry weight and expressed as pmol/s/mg dry weight.

Mitochondrial calcium retention capacity. Changes in extramitochondrial calcium concentration were monitored fluorometrically using Calcium Green (1 μM, excitation/emission 506/532 nm; Invitrogen, Waltham, Mass) as per manufacturer's instructions.

Citrate synthase activity assays. Activity assays were performed using a citrate synthase activity assay kit (Sigma-Aldrich, St. Louis, Mo) as per manufacturer's instructions.

Muscle contractile force measurements. Contractile force measurements were performed using isolated extensor digitorum longus (EDL) muscles as previously described.[23]

Total RNA and quantitative reverse transcription-polymerase chain reaction gene expression analysis. Total RNA was extracted from mouse EDL muscles using TRIzol (Invitrogen) and reverse-transcribed using SuperScript IV (Invitrogen). Quantitative reverse transcription-polymerase chain reaction (qRT-PCR) was performed using an ABI ViiA-7 system (Applied Biosystems, Waltham, Mass).

Statistics. Data are presented as a ratio of the treated (ischemic or CTX injected) left (L) to the untreated (non-ischemic or saline sham injected) contralateral control (R) limb and mean ± standard error of the mean. Force frequency and fiber phenotype data are presented as L and R for each strain with mean ± standard error of the mean. Statistical analyses were carried out using StatPlus:mac (version 2009; AnalystSoft, Walnut, Calif), Vassarstats (www.vassarstats.net), or Prism 6 (version 6.0d; Graphpad Software Inc, La Jolla, Calif) software. Two sided *t*-tests were performed a priori to determine mean differences in the control limbs of the strains. All other data were compared using Student two-tailed *t*-test or analysis of

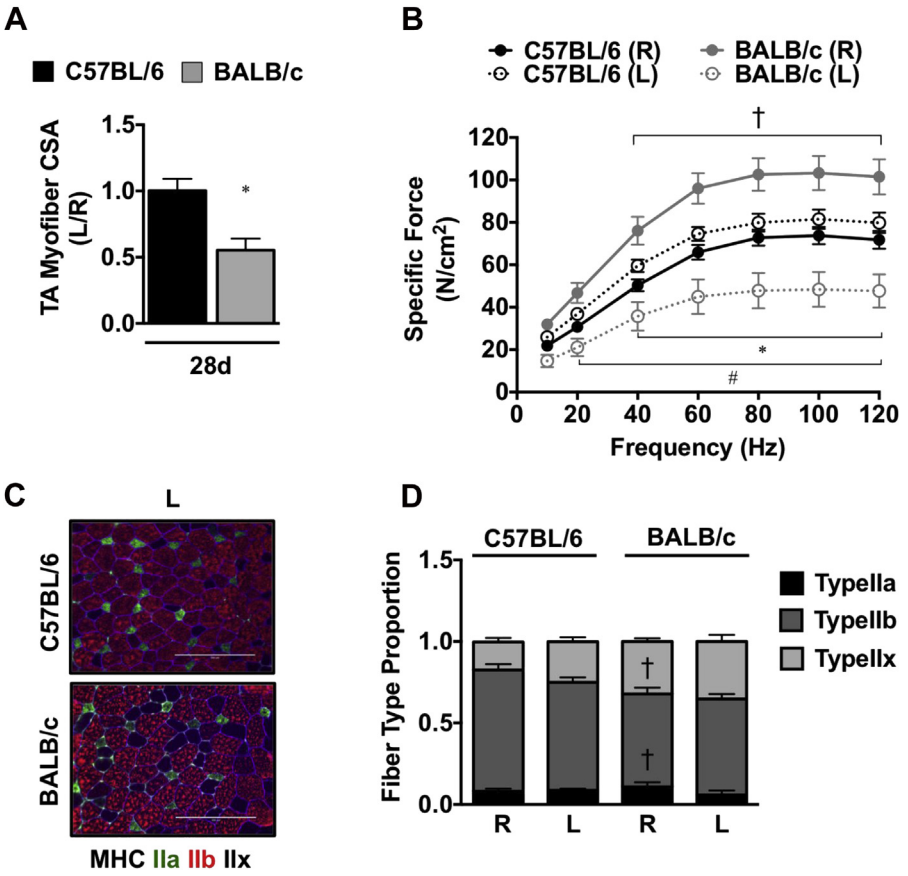

Fig 1. Muscle atrophy, morphology, and force production in ischemic hind limbs. Subacute femoral artery occlusion was performed on BL6 and BALB/c mice using placement of a single ameroid constrictor on the proximal portion of the femoral artery. **A,** Sections of tibialis anterior (*TA*) muscles were analyzed for myofiber cross-sectional area (*CSA*) and presented as the ratio of the ischemic limb (*L*) to the nonischemic contralateral control limb (*R*), mean ± standard error of the mean (SEM). * $P < .05$ vs C57BL/6. **B,** Force frequency curves were determined in isolated extensor digitorum longus (EDL) muscles from both strains at 28 postoperative days. * $P < .05$ vs day and strain matched R. † $P < .05$ vs day matched C57BL/6 R. # $P < .05$ vs day matched C57BL/6 L. **C,** Sections of EDL muscles were immunofluorescently labeled with selective myosin heavy chain antibodies to determine the proportion of each fiber type (IIa, IIb, IIx) present. The *scale bar* inlays are 200 μm in length. **D,** Myofiber phenotypes are presented as the relative proportions of each in the L and Rs, mean ± SEM. † $P < .05$ vs C57BL/6 R. All data are representative of n ≥ 6 per strain per time point.

variance with Holm-Sidak multiple comparison tests when applicable. In all cases, $P < .05$ was considered statistically significant.

RESULTS

Strain-dependent myopathy during subacute ischemia. To examine the functional outcomes of ischemic myopathy, we subjected genetically ischemia-resistant (C57BL/6) and ischemia susceptible (BALB/c) mice to subacute hind limb ischemia (SLI) for 7 and 28 days. Similar to our previous findings,[9] SLI resulted in large pockets of anucleate necrotic myofibers (Supplementary Fig 1, online only, *A* and *B*), fewer centralized nuclei and reduced total myofiber count (Supplementary Fig 1, online only, *C*) in BALB/c muscle compared with C57BL/6. Myofiber size (cross-sectional area) was significantly ($P = .007$) attenuated in BALB/c tibialis anterior (TA) muscle (Fig 1, *A*) after 28 days (d) of SLI, indicating atrophy associated with ischemic regeneration unique to this parental strain. BALB/c myofiber atrophy (cross-sectional area) was driven primarily by a decrease in myofiber size in the ischemic left limb (1258.0 ± 185.9 μm^2) and not increases in myofiber size of the contralateral control limb (2299.4 ± 172.4 μm^2) relative to the C57BL/6 ischemic (2345.6 ± 209.7 μm^2) and control (2362.2 ± 124.8 μm^2) limbs, respectively. qRT-PCR revealed differential patterns of expression in muscle atrophy F-box (Supplementary Fig 2, online only, *A*), MyoD family inhibitor (Supplementary Fig 2, online only, *B*), and muscle ring finger protein-1 (Supplementary Fig 2, *C*) messenger RNA (mRNA) between the strains after SLI.

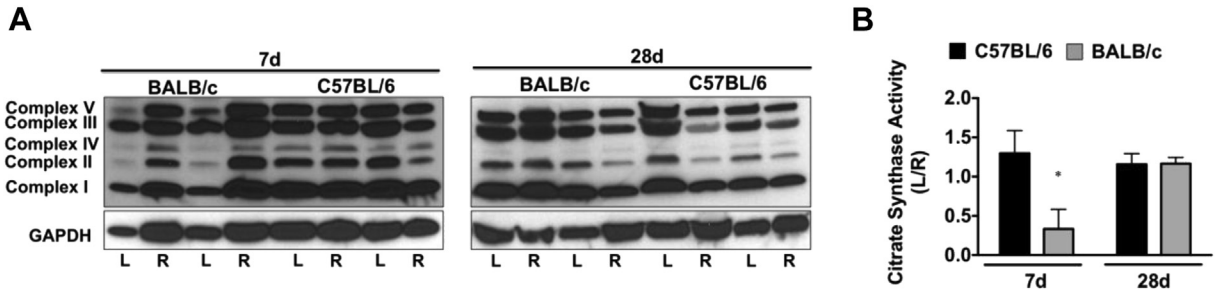

Fig 2. Parental strain effects on ischemic tissue mitochondrial content. Subacute femoral artery occlusion was performed on C57BL/6 and BALB/c mice using placement of a single ameroid constrictor on the proximal portion of the femoral artery, immediately proximal to the epigastric arterial branch. **A,** Western blot analysis for mitochondrial complex content was performed for qualitative observation of complex I to V protein abundances, with glyceraldehyde 3-phosphate dehydrogenase (*GAPDH*) protein blotting as a loading reference. **B,** Citrate synthase activity was determined in extensor digitorum longus (EDL) muscle as an indicator of muscle mitochondrial content. Data are representative of the ratio of the ischemic (*L*) to the nonischemic contralateral control (*R*) limb, mean ± standard error of the mean (SEM) and representative of n ≥ 6 per strain per time point. * $P < .05$ vs day matched C57BL/6. *d*, Days.

A priori analysis revealed an increase in force generation in the BALB/c contralateral control EDL compared with the C57BL/6 ($P < .05$; 40-120 Hz) after SLI. Specific force was uniquely decreased ($P < .05$) from the contralateral control in the BALB/c ischemic limb across multiple frequencies (40-120 Hz; Fig 1, *B*) and was similarly decreased ($P < .05$) from the C57BL/6 ischemic limb at multiple frequencies (20-120 Hz). Fiber typing (Fig 1, *C*) showed that BALB/c control EDL muscle possesses a slightly lower proportion of type IIb ($P = .009$) and greater proportion of type IIx ($P = .01$) than C57BL/6 control limb after SLI. Distributions of myosin heavy chain type in the ischemic limb were not significantly altered by SLI in either strain (Fig 1, *D*). Myosin heavy chain type I was detected similarly between the strains at a proportion of <1%.

TA muscles were stained with PR dye and imaged using a polarized light microscope (Supplementary Fig 3, online only, *A*). The birefringent properties of the PR dye lead to a color hue shift from green to yellow to orange to red with increasing thickness of the collagen molecules present in the tissue. Thin collagen trended toward increase ($P = .06$) after 7d SLI in BALB/c limbs (Supplementary Fig 3, online only, *B*) but was resolved by 28d. Thick collagen deposition was not altered between the strains at either 7d or 28d SLI (Supplementary Fig 3, online only, *C*). Similar to our previously reported findings for SLI,[9] capillary density ($CD31^+$ area; Supplementary Fig 3, online only, *D*) was altered correspondingly between strains after SLI (Supplementary Fig 3, online only, *E*). Oil Red-O staining was performed to identify muscle lipid accumulation (Supplementary Fig 4, online only, *A*), which was not different between the strains at 7d SLI, but trended ($P = .09$) toward an increase in BALB/c muscle (Supplementary Fig 4, online only, *B*). We verified differential intermuscular lipid deposition at 28d SLI with BODIPY (493/503; Supplementary Fig 4, online only, *C*). $BODIPY^+$ (493/503) inclusions were not statistically different between the strains after 28d SLI (Supplementary Fig 4, online only, *D*).

The innate and adaptive immune responses to injury are known to differ among inbred strains of mice.[24,25] We have previously characterized increased macrophage ($CD11b^+$) cell infiltration in BALB/c compared with C57BL/6 mice using immunofluorescence in ischemic skeletal muscle tissue at 7d after SLI.[9] To further investigate the role of the innate immune response to SLI we performed CD11b immunostaining on muscle tissue sections from both strains after 28d SLI (data not shown), however, we were unable to detect a positive signal. To confirm the presence of $CDllb^+$ cells in SLI tissue at both time points, we performed qualitative immunoblot analyses in EDL lysate from both strains after 7d and 28d of SLI (Supplementary Fig 5, online only, *A* and *B*). Positive signal was detected at 7d in both strains, but not at 28d. We also sought to characterize the mRNA expression changes of the proinflammatory cytokines tumor necrosis factor (TNF)α, interleukin (IL)1-β, and IL-6 of both strains in response to SLI using qRT-PCR. All three cytokines increased in both strains of mice after 7d SLI. No statistically significant differences were observed in cytokine mRNA expression between the strains at 7d SLI, although all three transcripts were acutely elevated. We observed differential patterns of expression in TNFα (Supplementary Fig 5, online only, *C*) and IL1-β (Supplementary Fig 5, online only, *D*), but not IL-6 (Supplementary Fig 5, online only, *E*) mRNA between the strains after 28d SLI.

Muscle mitochondrial content and respiratory functional abnormalities are strain-dependent during subacute limb ischemia. We examined whether alterations in muscle mitochondrial content occur after SLI. Western blot analysis for mitochondrial complex proteins (Fig 2, *A*) revealed a qualitative (7d) decrease in Complex I to V in BALB/c muscle, which was restored to contralateral control (R) levels by 28d SLI. Citrate synthase enzyme activity (a commonly used surrogate for mitochondrial content; Fig 2, *B*) was reduced ($P = .04$) in BALB/c limb muscle after 7d SLI, and recovered to C57BL/6 levels at 28d.

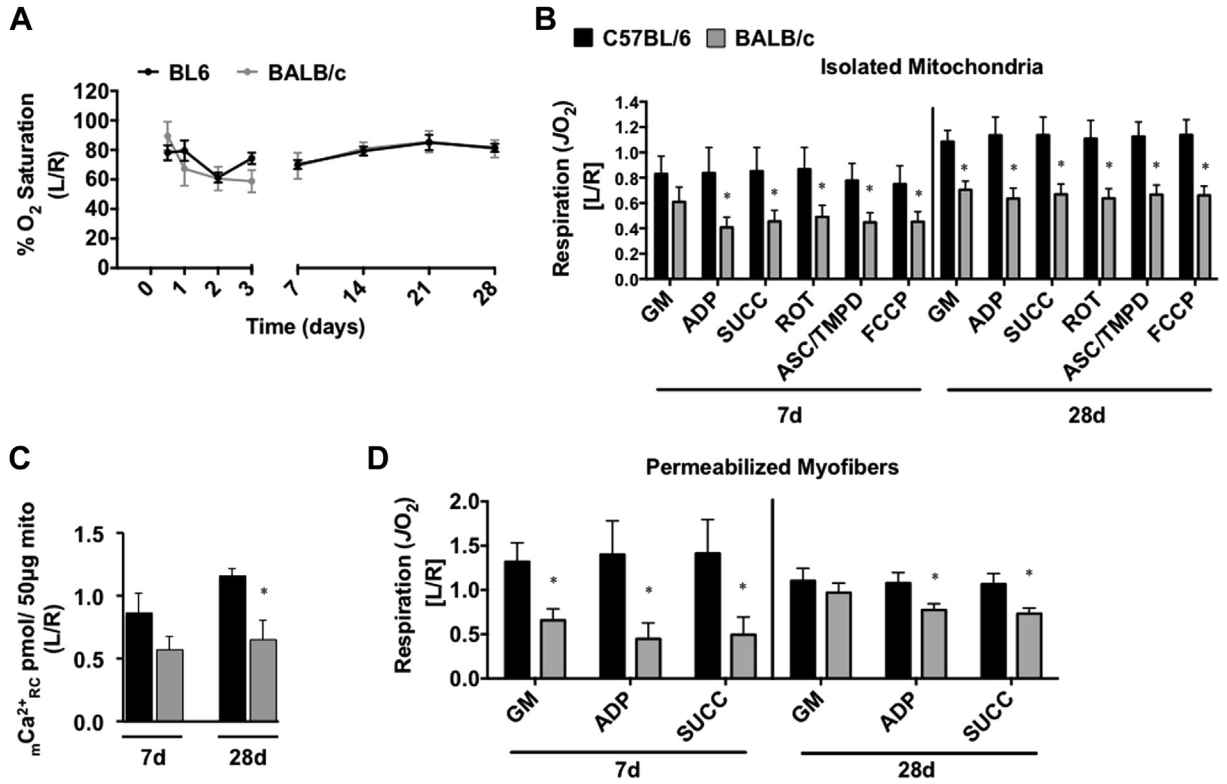

Fig 3. Limb muscle mitochondrial response to subacute hindlimb ischemia. **A,** Subacute femoral artery occlusion was performed on C57BL/6 (*BL6*) and BALB/c mice using placement of a single ameroid constrictor (1AC) on the proximal portion of the femoral artery, immediately proximal to the epigastric arterial branch. Paw tissue oxygen saturation (SO_2; *% O_2*), measured via white light reflectance spectroscopy, was analyzed to determine distal limb O_2. **B,** Mitochondrial respiration (oxygen consumption rate [JO_2], as a measure of electron transport system flux) was measured in isolated mitochondria using high-resolution respirometry. The respiratory states assessed were: (1) glutamate/malate supported state 2 respiration (*GM*); (2) glutamate/malate supported state 3 (*ADP*); (3) GM and succinate supported state 3 (*SUCC*); (4) succinate supported state 3 (*ROT*); (5) ascorbate/N,N,N′,N′-tetramethyl-p-phenylenediamine (*ASC/TMPD*); and (6) carbonyl cyanide-4-(trifluoromethoxy)phenylhydrazone supported uncoupled respiration (*FCCP*). **C,** Ca^{2+} retention capacity was measured in ischemic (*L*) and nonischemic contralateral control (*R*) mitochondria isolated from the limb plantar flexors (gastrocnemius, plantaris, and soleus) as a function of mitochondrial integrity and resistance to permeability transition. **D,** Oxygen consumption was also determined in saponin permeabilized myofiber bundles isolated from the gastrocnemius muscle. Data are representative of the ratio of the L to the R. * $P < .05$ vs C57BL/6. All data are mean ± standard error of the mean and representative of n ≥ 6 per strain per time point. *d,* Days.

SO_2, measured at the distal paw after SLI, was nearly identical between the strains at all time points measured (Fig 3, *A*). Mitochondrial respiratory capacity under multiple substrate conditions trended toward decreased values ($P < .10$ across all conditions except glutamate-malate) in ischemic BALB/c muscle mitochondria after 7d SLI (Fig 3, *B*) and significantly decreased ($P < .01$ across all conditions) at 28d SLI. To assess the sensitivity of the mitochondrial permeability transition pore, we performed a mitochondrial calcium retention capacity assay using the fluorophore Calcium Green-5N (Fig 3, *C*). BALB/c mitochondrial calcium retention capacity was significantly ($P = .007$) decreased at 28d SLI. To circumvent potential influences of isolating mitochondria,[26] we also assessed the respiratory function in saponin-permeabilized myofibers isolated from the gastrocnemius muscle. Respiratory capacity was comparatively lower at 7d and 28d SLI in BALB/c fiber bundles ($P < .05$ across all conditions, excluding glutamate-malate at 28d; Fig 3, *D*). Taken together, these data suggest that substantial skeletal muscle mitochondrial impairments exist in BALB/c limb muscle during SLI, but not in C57BL/6. In isolated mitochondria and permeabilized myofiber bundle models, it is thought that respiration is primarily driven by myofiber mitochondria. This assumption is made on the basis of the relatively low density of satellite and other interstitial cells in skeletal muscle and the low mitochondrial density of resident satellite cells.[27] Further, during the isolation process connective and fat tissues are removed both mechanically and by centrifugation.

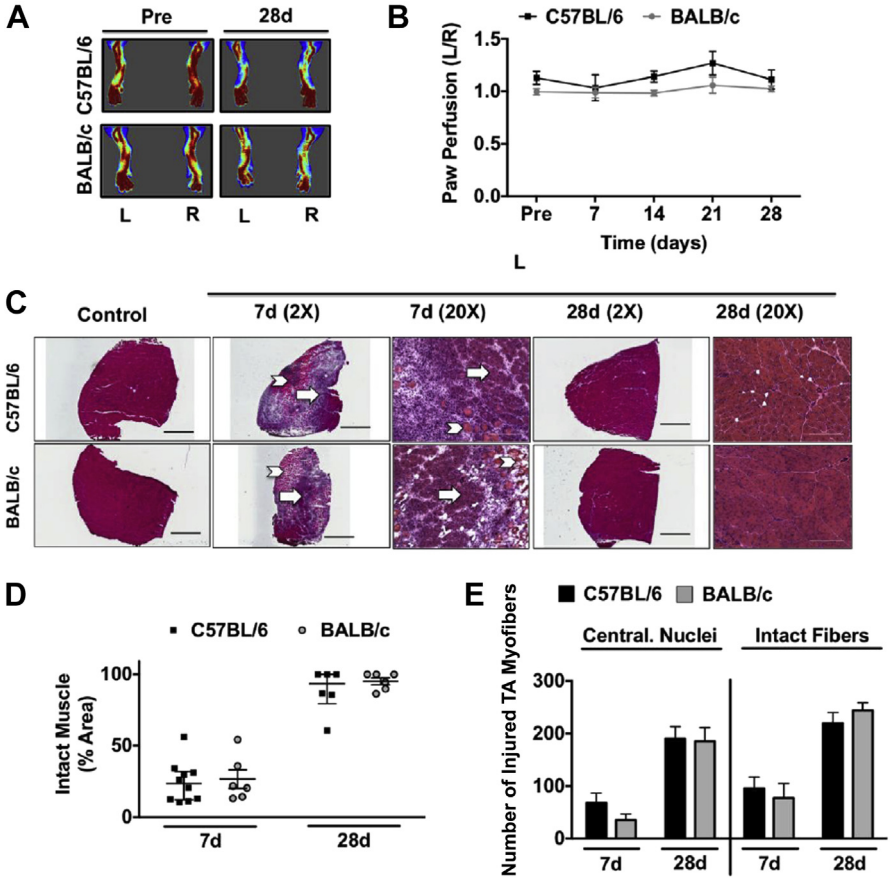

Fig 4. Strain independent myopathy with nonischemic myotoxin injury. Cardiotoxin (CTX) was injected intramuscularly into the tibialis anterior (*TA*) and the lateral/medial heads of the gastrocnemius muscle. A sham injection (*Control*) of equal volume sterile saline was injected in the same muscles in the contralateral control limb (*R*). **A,** Representative laser Doppler perfusion images of the paw before and during recovery from CTX injection. **B,** Quantification of blood flow in the hind paw, presented as the ratio of the CTX injected (*L*) limb to the R limb. **C,** The *scale bar* inlays are 1000 μm in length (2X), and 200 μm in length (20X). Representative 2X and 20X images of hematoxylin and eosin (H&E) stained sections of TA muscles 7 and 28 days (*d*) after CTX (L) injury. The *arrows* indicate intact muscle; *chevrons* indicate regions of anucleate necrotic fibers. **D,** Muscle regeneration was quantified from 2X H&E images by measuring the total regions of interest (*Area*) containing necrotic/anuclueate myofibers, which is represented by median and interquartile range. **E,** Total myofibers with centralized nuclei (*Central. Nuclei*) and total myofiber number (*Intact Fibers*) were determined in representative images taken with magnification ×10. All data are mean ± standard error of the mean and representative of n ≥ 6 per strain per time point. *Pre,* Baseline.

Strain-independent myopathy in nonischemic muscle regeneration. To test the regenerative response between strains to nonischemic muscle injury, we used intramuscular injection of CTX, which we verified as nonischemic using LDPI and tissue SO_2 measurements (Fig 4, *A* and *B*; Supplementary Fig 6, online only). H&E staining of TA muscles from 7d and 28d CTX revealed large pockets of anucleate necrotic myofibers accompanied by extensive mononuclear cell infiltration and the presence of small basophilic myofibers (Fig 4, *C* and *D*), centralized nuclei, and total intact fibers (Fig 4, *E*) in both strains. Myofiber size (cross-sectional area) was similarly altered in both strains (Fig 5, *A*) after 28d CTX. Because CTX was not directly injected into the EDL, but EDL muscles were used for force measurements in this study, EDL and TA muscles were isolated 24 hours after CTX and visualized using H&E to confirm the extent of injury in both (Supplementary Fig 7, online only).

Force frequency relationships in isolated EDL muscles (Fig 5, *B*) were also unaffected by parental strain and completely recovered to contralateral control values by 28d CTX. Notably, there was no increase in force generation in the BALB/c control EDL after CTX. Fiber typing (Fig 5, *C*) revealed that, in the absence of ischemic insult, the contralateral control EDL muscles of C57BL/6 and BALB/c mice possess similar distributions of MyHC (Fig 5, *D*). After CTX, the proportion of IIb myofibers was modestly increased ($P = .03$) in the injured BALB/c

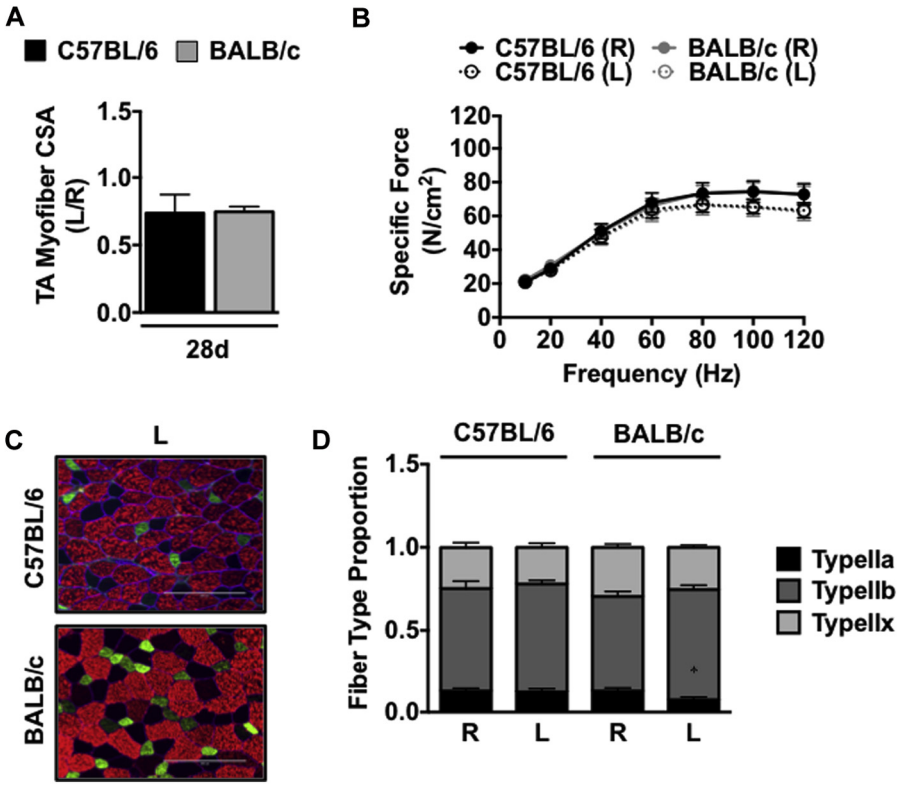

Fig 5. Muscle atrophy, morphology, and force production after a nonischemic injury. Nonischemic muscle regeneration was induced by cardiotoxin (CTX) injection. **A,** Sections of tibialis anterior (*TA*) muscles were analyzed for myofiber cross-sectional area (*CSA*) and presented as the ratio of the CTX-injected (*L*) to the contralateral control (*R*) limb; mean ± standard error of the mean (SEM). **B,** Force frequency curves were determined in isolated extensor digitorum longus (EDL) muscles from both strains at 28 postoperative days. **C,** Sections of EDL muscles were immunofluorescently labeled with selective myosin heavy chain antibodies to determine the proportion of each fiber type (IIa, IIb, IIx) present. The *scale bar* represents 200 μm in length. **D,** * $P < .05$ vs strain matched R. All data are mean ± SEM and representative of n ≥ 6 per strain per time point.

EDL compared with the contralateral control. MyHC type I was detected similarly between strains in a proportion of <1%. Taken together, these data suggest that muscle regeneration in a model of nonischemic myofiber injury occurs similarly between C57BL/6 and BALB/c mice.

Muscle fibrosis after CTX was analyzed using PR dye (Supplementary Fig 8, online only, *A*). Thin collagen was increased to a greater extent ($P = .03$) in BALB/c limb muscle after 7d CTX and trended ($P = .07$) toward significance at 28d CTX (Supplementary Fig 8, online only, *B*). Limb muscle thick collagen deposition was altered similarly in both parental strains after CTX (Supplementary Fig 8, online only, *C*). Capillary density (Supplementary Fig 8, online only, *D*) was similarly altered after CTX (Supplementary Fig 8, online only, *E*). Lipid accumulation (Oil Red-O staining) in BALB/c limb muscle trended toward an increase ($P = .07$) from C57BL/6 at 7d CTX in BALB/c muscle but was similarly altered between the strains at 28d CTX (Supplementary Fig 9, online only, *A* and *B*). Strain-specific lipid positive inclusions, assessed using BODIPY (493/503), were similarly altered after 28d CTX (Supplementary Fig 9, online only, *C* and *D*).

Muscle mitochondrial content and respiratory function are strain-independent during nonischemic regeneration. Western blot analyses for mitochondrial complex proteins (Fig 6, *A*) qualitatively showed varying alterations in mitochondrial complex abundances after 7d CTX, which were stabilized at 28d CTX. Citrate synthase activity (Fig 6, *B*) was unchanged between the parental strains after 28d CTX. Paw SO_2 was similar between the strains at all time points (Fig 7, *A*). Mitochondrial Ca^{2+} retention capacity (Fig 7, *C*) was altered equally between the strains after CTX. Mitochondrial respiratory capacity (high-resolution respirometry) increased ($P < .004$ across glutamate/malate supported state 3, ascorbate/N,N,N′,N′-tetramethyl-p-phenylenediamine (TMPD), and carbonyl cyanide-4-(trifluoromethoxy)phenylhydrazone) uncoupled respiration in the injured BALB/c mitochondria after 7d CTX (Fig 7, *B*), but was returned to baseline at 28d CTX. Taken together these data suggest that, in the absence of

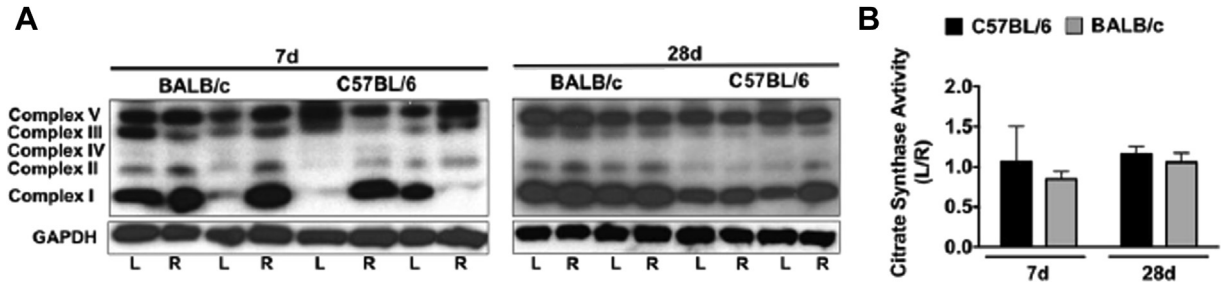

Fig 6. Muscle mitochondrial content after a nonischemic injury. Nonischemic muscle regeneration was induced with cardiotoxin (CTX) injection. **A,** Western blot analysis for mitochondrial complex content was performed for qualitative observation of complex I to V protein abundances, with glyceraldehyde 3-phosphate dehydrogenase (*GAPDH*) protein blotting as a loading reference. **B,** Citrate synthase activity was determined in extensor digitorum longus (EDL) muscle as an indicator of muscle mitochondrial content. Data are representative of the ratio of the CTX-injected (*L*) to the contralateral control (*R*) limb; mean ± standard error of the mean, and representative of n ≥ 6 per strain per time point. *d,* Days.

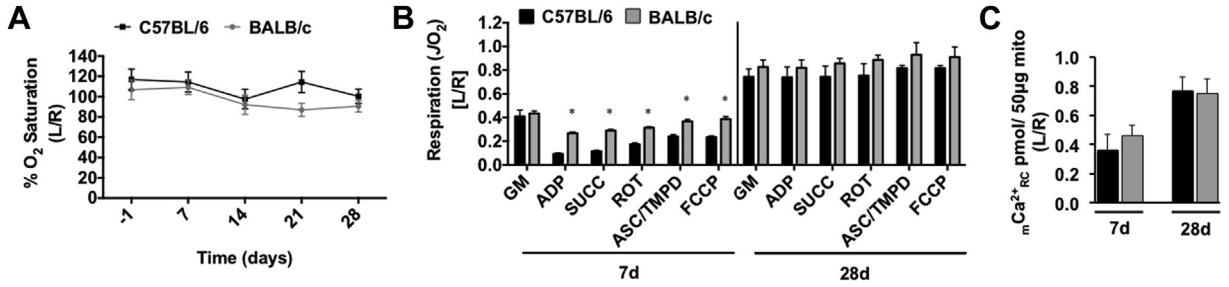

Fig 7. Limb muscle mitochondrial response to nonischemic injury. Nonischemic muscle regeneration was induced by cardiotoxin (CTX) injection. **A,** Paw tissue oxygen saturation (SO_2; *% O_2*), measured via white light reflectance spectroscopy, was analyzed to determine distal limb O_2. **B,** Mitochondrial respiration (oxygen consumption rate [JO_2], as a measure of electron transport system flux) was measured in isolated mitochondria using high-resolution respirometry. The respiratory states assessed were: (1) glutamate/malate supported state 2 respiration (*GM*); (2) glutamate/malate supported state 3 (*ADP*); (3) GM and succinate supported state 3 (*SUCC*); (4) succinate supported state 3 (*ROT*); (5) ascorbate/N,N,N′,N′-tetramethyl-p-phenylenediamine (*ASC/TMPD*); and (6) carbonyl cyanide-4-(trifluoromethoxy) phenylhydrazone supported uncoupled respiration. Data are representative of the ratio of the CTX-injected limb (*L*) to the contralateral control limb (*R*). **P* < .05 vs day matched C57BL/6. **C,** Ca^{2+} retention capacity was measured in L and R limb mitochondria isolated from the plantar flexors (gastrocnemius, plantaris, and soleus) as a function of mitochondrial integrity and resistance to permeability transition. Data are representative of the ratio of the L to the R limb; mean ± standard error of the mean, and representative of n ≥ 6 per strain per time point.

ischemia, regenerating limb muscle mitochondrial content and respiratory capacity are unaffected by parental strain.

DISCUSSION

In this study, we found that the ability of limb muscle to regenerate from an injury that does not involve reduced limb blood flow or attenuated SO_2 is parental strain-independent, at least with regard to ischemia-divergent C57BL/6 and BALB/c mice. Regeneration from ischemic insult, however, results in contractile force deficits that correspond with muscle wasting, delayed myofiber regeneration, and mitochondrial dysfunction genetically inherent to the limb muscles of the ischemia-susceptible BALB/c parental strain. In our previous description of ameroid constrictor-induced subacute limb ischemia we determined that muscle myopathy (atrophy, regenerative deficits) occurred independent of strain-specific alterations in muscle vascular density.[9] In this study, we showed the functional, morphological, and bioenergetic consequences of strain-dependent ischemic myopathy. Despite SO_2 similar to C57BL/6 and a lack of tissue necrosis, the mitochondria and myofiber contractile apparatus of the BALB/c limb muscle remain dysfunctional long after the onset of the ischemic insult. Although the degenerative insult might be initially caused by occlusive obstruction of blood flow to the limb, the inability to recover muscle mass and function might involve deficits genetically inherent to the

muscle myofibers. Our results also show, in a refined and subacute preclinical PAD model, that ischemic muscle mitochondrial respiration is uniquely affected by parental strain genetics. This finding supports the notion that the plasticity of ischemic muscle is a critical determinant of the manifestation of limb pathology and lends credence to the mitochondrion as an organelle intimately involved in the failure to recover from PAD.

Ameroid constrictors have been used in mice to more closely mimic the chronic nature of human CLI[28] in the absence of the rapid necrosis that occurs with acute hindlimb ischemia. We previously validated this model as subacute in nature and insufficient in severity to cause a complete cessation of blood flow, assessed using LDPI.[9] To verify a lack of strain-dependent differences in tissue oxygen, we paralleled our LDPI data with SO_2 measurements. Light-guided spectrophotometry measurements, in conjunction with flow analysis, have been used in patients with CLI before and after revascularization to provide ischemic limb SO_2 and indicate the functionality of tissue blood flow.[29] In this study, SO_2 measurements provided verification of the nonischemic nature of the CTX insult in our experiments. Importantly, paw SO_2 measurements during SLI further indicate that tissue oxygenation might not be a strain-dependent limiting factor in this model of PAD. This speaks to the unique nature of SLI, which results in blood flow of at least 40%[9,28] and SO_2 values of 60% of control in the ischemic limb. These levels appear to be sufficient to overcome any substantial differences in strain-dependent vascularity (collateral vessel density)[1,2,7,30] or blood flow and prevent tissue loss during SLI. They are not, however, sufficient to prevent sustained deficits in muscle function and mitochondrial respiration. This points to inherent deficits in the BALB/c muscle response to decreased blood flow and SO_2 that result in a sustained functional impairment.

Muscle function, measured using exercise testing, is an important indicator of morbidity and mortality in PAD patients,[31-33] and alterations in muscle force production due to morphological adaptations to ischemia could have severe negative consequences for patient outcomes. The use of a genetically ischemia-susceptible parental strain (BALB/c) in this work is intended to be analogous with the clinical population most susceptible to ischemic pathology (ie, CLI patients). Previous studies have suggested that a BALB/c strain-dependent impairment of the myogenic response to injury exists.[34-37] Interestingly, the injury models used in these studies often contain a remote or local ischemic component (eg, crush injury, tissue explants). Our CTX data could suggest that, before the development of occlusive limb ischemia, the lack of outward susceptibility of some patients to myopathies might not accurately predict the severity of PAD manifestation. Even in the absence of superficial tissue necrosis, BALB/c mice display significant myopathies and functional deficits when ischemia is present. Clinically, restoring flow to the ischemic limb has provided little alleviation of morbidity and mortality outcomes in CLI patients,[10,38,39] and might be indicative of an unexplored inherent susceptibility of the limb muscle tissue of these patients to ischemia.

The maintenance of mitochondrial function in ischemic skeletal muscle is a potential major contributor to tissue pathology for two primary reasons: (1) reduced adenosine triphosphate generation can alter ion homeostasis and contribute to the activation of the mitochondrial permeability transition pore and initiation of apoptosis; and (2) substantial degeneration and regeneration in the ischemic muscle environment requires efficient electron transport flux to satisfy the high demand for adenosine triphosphate production and the efficient performance of these tasks. BALB/c limb muscle mitochondria exhibit an extreme respiratory capacity reduction (approximately 40%-60% compared with the control limb); whereas mitochondrial respiratory capacity in C57BL/6 mice is unaffected. It is conceivable that the bioenergetic demand outpaces energy production in ischemic BALB/c tissues, thus contributing to an inefficient or incomplete regenerative process. A previous study[16] showed, in genetically ischemia resistant C57BL/6 mice, that chronic (12-week) limb ischemia results in significant reductions in electron transport flux and oxidative damage and histological signs of myopathy despite increased mitochondrial content. Unfortunately, the use of acute hindlimb ischemia makes these findings difficult to compare with the data we obtained using the SLI model. A common theme, however, is that reduced skeletal muscle mitochondrial function might be a mechanism underlying the increased susceptibility to ischemic myopathies in these mice. Little is known about the effect of parental strain genetics on the ischemic mitochondrial genome or proteome. Future studies are warranted to identify specific mitochondrial targets for which to test therapeutics preclinically. Mitochondria provide an attractive target for therapeutic intervention because of their density in skeletal muscle and roles in the generation and maintenance of energy and redox state,[40,41] potentially gatekeeping the function and mortality of ischemic muscle myofibers during regeneration from ischemic injury.

The findings presented in this study are a logical "next step" to our previous observations of a strain-dependent manifestation of histological pathology during ischemia.[8,9] Of particular interest is the ischemic context-dependent nature of mitochondrial respiratory abnormalities between ischemia resistant (C57BL/6) and ischemia susceptible (BALB/c) strains of mice. No differences in mitochondrial respiration were observed between the contralateral limbs of the parental strains or after CTX injury. Ischemia, however, caused a clear segregation in electron transport flux defined by significantly impaired mitochondrial respiratory capacity in BALB/c muscle. Collectively, our results suggest that a potential component of the ischemic myopathy that occurs in the BALB/c strain is an inability to handle the bioenergetic demands of limb skeletal muscle degenerative/regenerative processes. A local oxidant rich environment devoid of properly functioning mitochondria could also perpetuate a cycle of tissue degeneration and

necrosis in a manner similar to the "crippled mitochondria" phenomenon, whereby suppressed mitochondrial function and reactive oxygen species generation lead to progressive cellular damage.

CONCLUSIONS

The results of this study show that genetic background is a critical determinant of the muscle functional outcome after subacute limb ischemia. The specific combination of surgical model and inbred strains of mice used in this study allowed us to show a muscle myofiber-specific mitochondrial respiratory component of ischemic myopathy that corresponds with functional deficits in muscle force production in BALB/c mice. These findings provide important insight into the genetic susceptibility of muscle force production and mitochondrial electron transport chain flux to limb ischemia, which is particularly important because of the role of muscle functional measures in predicting PAD manifestation and patient outcomes. These findings could lead to novel therapies targeted directly at the skeletal muscle myofibers of the peripheral limb, which could be used alone or in combination with reperfusion strategies to improve clinical care.

The authors thank Dr Ken Soderstrom and Khoa Do for their technical expertise and assistance.

AUTHOR CONTRIBUTIONS

Conception and design: CS, TR, TG, JB, JM
Analysis and interpretation: CS, TR, CL, ES, JM
Data collection: CS, TR, CL, MI, TG, JB, ES, JM
Writing the article: CS, TR, CL, TG, ES, JM
Critical revision of the article: CS, TR, MI, TG, ES, JM
Final approval of the article: CS, TR, CL, MI, TG, JB, ES, JM
Statistical analysis: CS, TR, ES, JM
Obtained funding: JB, JM
Overall responsibility: JM

REFERENCES

1. Chalothorn D, Clayton JA, Zhang H, Pomp D, Faber JE. Collateral density, remodeling, and VEGF-A expression differ widely between mouse strains. Physiol Genomics 2007;30:179-91.
2. Chalothorn D, Faber JE. Strain-dependent variation in collateral circulatory function in mouse hindlimb. Physiol Genomics 2010;42:469-79.
3. Dokun AO, Keum S, Hazarika S, Li Y, Lamonte GM, Wheeler F, et al. A quantitative trait locus (LSq-1) on mouse chromosome 7 is linked to the absence of tissue loss after surgical hindlimb ischemia. Circulation 2008;117:1207-15.
4. Katwal AB, Dokun AO. Peripheral arterial disease in diabetes: is there a role for genetics? Curr Diab Rep 2011;11:218-25.
5. Matzke S, Lepantalo M. Claudication does not always precede critical leg ischemia. Vasc Med 2001;6:77-80.
6. Wang S, Zhang H, Dai X, Sealock R, Faber JE. Genetic architecture underlying variation in extent and remodeling of the collateral circulation. Circ Res 2010;107:558-68.
7. Wang S, Zhang H, Wiltshire T, Sealock R, Faber JE. Genetic dissection of the Canq1 locus governing variation in extent of the collateral circulation. PLoS One 2012;7:e31910.
8. McClung JM, McCord TJ, Keum S, Johnson S, Annex BH, Marchuk DA, et al. Skeletal muscle-specific genetic determinants contribute to the differential strain-dependent effects of hindlimb ischemia in mice. Am J Pathol 2012;180:2156-69.
9. McClung JM, McCord TJ, Southerland K, Schmidt CA, Padgett ME, Ryan TE, et al. Subacute limb ischemia induces skeletal muscle injury in genetically susceptible mice independent of vascular density. J Vasc Surg 2016;64:1101-11.
10. Hammer A, Steiner S. Gene therapy for therapeutic angiogenesis in peripheral arterial disease - a systematic review and meta-analysis of randomized, controlled trials. Vasa 2013;42:331-9.
11. Bhat HK, Hiatt WR, Hoppel CL, Brass EP. Skeletal muscle mitochondrial DNA injury in patients with unilateral peripheral arterial disease. Circulation 1999;99:807-12.
12. Brass EP, Hiatt WR. Acquired skeletal muscle metabolic myopathy in atherosclerotic peripheral arterial disease. Vasc Med 2000;5:55-9.
13. Brass EP, Hiatt WR, Green S. Skeletal muscle metabolic changes in peripheral arterial disease contribute to exercise intolerance: a point-counterpoint discussion. Vasc Med 2004;9:293-301.
14. Brass EP, Wang H, Hiatt WR. Multiple skeletal muscle mitochondrial DNA deletions in patients with unilateral peripheral arterial disease. Vasc Med 2000;5:225-30.
15. Pipinos II, Judge AR, Zhu Z, Selsby JT, Swanson SA, Johanning JM, et al. Mitochondrial defects and oxidative damage in patients with peripheral arterial disease. Free Radic Biol Med 2006;41:262-9.
16. Pipinos II, Swanson SA, Zhu Z, Nella AA, Weiss DJ, Gutti TL, et al. Chronically ischemic mouse skeletal muscle exhibits myopathy in association with mitochondrial dysfunction and oxidative damage. Am J Physiol Regul Integr Comp Physiol 2008;295:R290-6.
17. Ryan TE, Schmidt CA, Green TD, Brown DA, Neufer PD, McClung JM. Mitochondrial regulation of the muscle microenvironment in critical limb ischemia. Front Physiol 2015;6:336.
18. Institute of Laboratory Animal Resources, Commission on Life Sciences, National Research Council. Guide for, the Care and Use of Laboratory Animals. Washington, DC: National Academy Press; 1996.
19. Yan Z, Choi S, Liu X, Zhang M, Schageman JJ, Lee SY, et al. Highly coordinated gene regulation in mouse skeletal muscle regeneration. J Biol Chem 2003;278:8826-36.
20. McClung JM, Van Gammeren D, Whidden MA, Falk DJ, Kavazis AN, Hudson MB, et al. Apocynin attenuates diaphragm oxidative stress and protease activation during prolonged mechanical ventilation. Crit Care Med 2009;37:1373-9.
21. Lark DS, Reese LR, Ryan TE, Torres MJ, Smith CD, Lin CT, et al. Protein kinase A governs oxidative phosphorylation kinetics and oxidant emitting potential at complex I. Front Physiol 2015;6:332.
22. Perry CG, Kane DA, Lin CT, Kozy R, Cathey BL, Lark DS, et al. Inhibiting myosin-ATPase reveals a dynamic range of mitochondrial respiratory control in skeletal muscle. Biochem J 2011;437:215-22.
23. Spangenburg EE, Le Roith D, Ward CW, Bodine SC. A functional insulin-like growth factor receptor is not necessary for load-induced skeletal muscle hypertrophy. J Physiol 2008;586:283-91.
24. Pulendran B, Smith JL, Caspary G, Brasel K, Pettit D, Maraskovsky E, et al. Distinct dendritic cell subsets differentially regulate the class of immune response in vivo. Proc Natl Acad Sci U S A 1999;96:1036-41.
25. Scalzo AA, Fitzgerald NA, Wallace CR, Gibbons AE, Smart YC, Burton RC, et al. The effect of the Cmv-1 resistance gene, which is linked to the natural killer cell gene complex, is mediated by natural killer cells. J Immunol 1992;149:581-9.
26. Picard M, Taivassalo T, Ritchie D, Wright KJ, Thomas MM, Romestaing C, et al. Mitochondrial structure and function are disrupted by standard isolation methods. PLoS One 2011;6:e18317.
27. Almada AE, Wagers AJ. Molecular circuitry of stem cell fate in skeletal muscle regeneration, ageing and disease. Nat Rev Mol Cell Biol 2016;17:267-79.
28. Yang Y, Tang G, Yan J, Park B, Hoffman A, Tie G, et al. Cellular and molecular mechanism regulating blood flow recovery in acute versus gradual femoral artery occlusion are distinct in the mouse. J Vasc Surg 2008;48:1546-58.
29. Rother U, Kapust J, Lang W, Horch RE, Gefeller O, Meyer A. The angiosome concept evaluated on the basis of microperfusion in critical

limb ischemia patients-an oxygen to see guided study. Microcirculation 2015;22:737-43.
30. Sealock R, Zhang H, Lucitti JL, Moore SM, Faber JE. Congenic fine-mapping identifies a major causal locus for variation in the native collateral circulation and ischemic injury in brain and lower extremity. Circ Res 2014;114:660-71.
31. McDermott MM, Guralnik JM, Ferrucci L, Tian L, Pearce WH, Hoff F, et al. Physical activity, walking exercise, and calf skeletal muscle characteristics in patients with peripheral arterial disease. J Vasc Surg 2007;46:87-93.
32. McDermott MM, Hoff F, Ferrucci L, Pearce WH, Guralnik JM, Tian L, et al. Lower extremity ischemia, calf skeletal muscle characteristics, and functional impairment in peripheral arterial disease. J Am Geriatr Soc 2007;55:400-6.
33. McGuigan MR, Bronks R, Newton RU, Sharman MJ, Graham JC, Cody DV, et al. Muscle fiber characteristics in patients with peripheral arterial disease. Med Sci Sports Exerc 2001;33:2016-21.
34. Grounds MD, McGeachie JK. A comparison of muscle precursor replication in crush-injured skeletal muscle of Swiss and BALBc mice. Cell Tissue Res 1989;255:385-91.
35. McGeachie JK, Grounds MD. Retarded myogenic cell replication in regenerating skeletal muscles of old mice: an autoradiographic study in young and old BALBc and SJL/J mice. Cell Tissue Res 1995;280:277-82.
36. Mitchell CA, Grounds MD, Papadimitriou JM. The genotype of bone marrow-derived inflammatory cells does not account for differences in skeletal muscle regeneration between SJL/J and BALB/c mice. Cell Tissue Res 1995;280:407-13.
37. Roberts P, McGeachie JK, Grounds MD. The host environment determines strain-specific differences in the timing of skeletal muscle regeneration: cross-transplantation studies between SJL/J and BALB/c mice. J Anat 1997;191:585-94.
38. Annex BH. Therapeutic angiogenesis for critical limb ischaemia. Nat Rev Cardiol 2013;10:387-96.
39. Cooke JP, Losordo DW. Modulating the vascular response to limb ischemia: angiogenic and cell therapies. Circ Res 2015;116:1561-78.
40. Karch J, Molkentin JD. Regulated necrotic cell death: the passive aggressive side of Bax and Bak. Circ Res 2015;116:1800-9.
41. Shirihai OS, Song M, Dorn GW 2nd. How mitochondrial dynamism orchestrates mitophagy. Circ Res 2015;116:1835-49.

Submitted Feb 23, 2016; accepted Apr 17, 2016.

Additional material for this article may be found online at www.jvascsurg.org.

APPENDIX (online only).

Supplementary methods

Animals. Experiments were conducted on adult (12- to 16-week-old) C57BL/6J (n = 33) or BALB/cJ (n = 36) mice. All work was approved by the Institutional Review Committee of East Carolina University. Animal care was in compliance with the *Guide for the Care and Use of Laboratory Animals.*[18] Subacute ischemia was performed as previously described,[1] with the following modifications. Mice were anesthetized using intraperitoneal injection of ketamine (90 mg/kg) and xylazine (10 mg/kg) and an ameroid constrictor (0.25 mm internal diameter; Research Instruments SW, Escondido, Calif) was placed on the femoral artery immediately distal to the lateral circumflex femoral artery and proximal to the origin of the superficial caudal epigastric artery. The inferior epigastric, lateral circumflex, and superficial epigastric artery branches of the femoral artery were left intact to preserve collateral perfusion to the limb. The CTX model of mouse muscle regeneration was performed as previously described[2] using 20-μL intramuscular injections of 5 μM *Naja nigricollis* venom into the TA, medial, and lateral heads of the gastrocnemius with a 27-gauge needle while the mice were anesthetized. An equivalent volume sham injection of 1× PBS was administered to the muscles of the contralateral hind limb. Because CTX was not directly injected into the EDL, but EDL muscles were used for various measurements in this study, a test animal (C57BL/6) was sacrificed 24 hours after TA injection of CTX and the EDL muscle was isolated and histologically stained to confirm that the extent of injury was identical to the TA muscle.

Assessment of limb perfusion and tissue SO_2. Limb blood flow was measured using LDPI as previously described[1] with the following modifications. Imaging was performed at a 4 ms/pixel scan rate on animals placed on a 37°C warming pad in the prone position using ketamine/xylazine anesthesia, and a Moor Instruments LDI2-High Resolution (830 nM) System up to 28 days after the intervention. Hind limb hair was removed with depilatory cream 24 hours before initial scanning and hair was removed with a microshaver at all other time points. Images were analyzed using the MoorLDI Image Review software (Moor Instruments). SO_2 was assessed at the aforementioned time points using a moorVMS-OXY white light spectrometer with a CPT-300 optical probe (Moor Instruments). SO_2 measurements were taken immediately after LDPI imaging for each animal to minimize positional variation. The optical probe was placed on the ventromedial region of the paw (SLI, CTX), as well as the TA and lateral head of the gastrocnemius muscle (CTX). Stable signal was collected for 10 seconds. Data were analyzed using the Moor VMS review software (Moor Instruments). Results for both analyses were expressed as a ratio of the treated limb to the untreated (SLI) or sham injected (CTX) contralateral limb.

Primary antibodies and histological stains. The following commercial antibodies were used: CD31 (AbD Serotec, Raleigh, NC, MCA-1364), dystrophin (Thermo Fisher Scientific; RB-9024), total oxphos (110413; Abcam, Cambridge, Mass), MyHC type I (BA-D5; Developmental Studies Hybridoma Bank, Iowa City, Iowa), MyHC type IIa (SC-71; Developmental Studies Hybridoma Bank, University of Iowa), MyHC type IIb (BF-F3; Developmental Studies Hybridoma Bank, University of Iowa), and CD11b (Abcam; 52478). 4′,6-diamidino-2-phenylindole (DAPI) mounting medium (H-1200; Vector Laboratories, Youngstown, Ohio) was also used. Histological stains were obtained from Sigma-Aldrich: Mayer hematoxylin, F8775; Direct red 80 (sirius red), MHS16; Picric acid, P6744; Weigert hematoxylin, HT1079.

IF and histology. Transverse sections (8-μm thick; 12-μm thick for Oil Red-O) from TA frozen in liquid nitrogen-cooled isopentane in optimum cutting temperature medium were cut using a Leica 3050S cryotome (Leica Biosystems) and collected on charged slides for staining. For morphological analyses, standard methods for H&E, Oil Red-O (intramuscular lipids), and PR (collagen) histological staining were performed. Analysis of muscle regeneration was performed on whole image transverse sections compiled from tiled H&E images at magnification ×40 using an Aperio CS2 digital slide analyzer (Leica Biosystems, Wetzlar, Germany) and the Aperio imagescope software (version 12.0, default settings; Leica Biosystems). Sections were segregated into regions of interest using morphology representative of tissue regeneration. Regions of interest were traced by a blinded investigator using the following categories: regenerating, intact myofibers with peripheral nuclei and/or small basophilic myofibers with centralized nuclei and low to moderate granulation tissue; and nonregenerating, granulation tissue with few to no basophilic myofibers and/or anucleate necrotic fibers. Muscle tissue morphology was presented as a percentage of the total muscle area including intact fibers and fascicular structure, the total number of myofibers, and the total number of myofibers with centralized nuclei. Analysis of lipid content was performed on 12-μm sections rinsed in 60% ethanol and stained in Oil Red-O (3 volumes of 1 g per 100 mL Oil Red-O in 99% isopropyl alcohol, in two volumes of 1% dextrin) for 20 minutes. Slides were then counterstained in Mayer hematoxylin and washed before coverslipping with a glycerol gelatin mounting medium at 37°C. Brightfield images at magnification ×10 were obtained and lipid positive staining was quantified by a blinded investigator using ImageJ (version 1.49; National Institutes of Health, Bethesda, Md) by thresholding hue, saturation, and brightness color spaces and measuring the percent area of lipid-positive stain within the field of view. Upper and lower threshold bounds were kept constant among all images analyzed. Collagen deposition was quantified using PR. Slides were allowed to come to room temperature (RT) and stained in Weigert hematoxylin solution for 10 minutes and were then rinsed in circulating tap water for 10 minutes. Slides were then

stained in a working solution of PR (sirius red 0.5 g per 500 mL, saturated picric acid 500 mL) for 1 hour and washed in acidified water before dehydration in ethanol, clearance in xylene, and mounting using glycerol gelatin at 37°C. Images at magnification ×10 were taken using an Olympus BX51-P polarized light microscope (Tokyo, Japan) and collagen deposition was quantified by a blinded investigator using ImageJ (version 1.49; National Institutes of Health) by thresholding hue, saturation, and brightness color space and measuring the percent area of the field of view occupied by each of two birefringent hue categories: red/orange and yellow/green. Upper and lower bounds for thresholding were kept constant among all images analyzed. To assess the relative distributions of muscle interstitial cells with lipid positive inclusions, transverse sections were prepared as described previously with the exception of fixation. The unfixed sections were immunostained for dystrophin as described previously for use as a counterstain. Sections were then stained with 1 μg/mL BODIPY 493/503 (Thermo Fisher Scientific) in 1× PBS diluent for 30 minutes. Slides were then mounted in Vectashield hard mount medium with DAPI and imaged as described previously. Image quantification was performed on representative images at magnification ×10 by a blinded investigator using ImageJ (version 1.49; National Institutes of Health) by decomposing the images into red-blue-green color space, setting appropriate standard threshold value limits, and measuring the percent area of BODIPY-positive stain within each image.

Vascular density and morphology IF was performed as previously described.[1,3] Briefly, transverse sections were allowed to come to RT and were fixed/permeabilized with ice-cold 1:1 acetone/methanol for 10 minutes at 4°C. Fixed sections were allowed to air dry for 5 minutes at RT and rehydrated in 1× PBS before blocking in 5% normal goat serum (Sigma-Aldrich) in 1× PBS at RT for 45 minutes. Slides were then incubated overnight at 4°C in a primary antibody solution. Slides were washed three times in 1× PBS at RT and incubated for 1 hour at RT in the dark in a secondary solution containing a 1:250 dilution of Alexa Fluor 488, or 647 conjugated secondary antibodies in blocking solution. Sections were washed in the dark three times for 5 minutes each with 1× PBS at RT, and coverslips were mounted using Vectashield HardSet Mounting Medium with DAPI (Vector Laboratories; H-1500). Images were captured using a Life Technologies Evos auto FL wide field fluorescence microscope (Thermo Fisher Scientific) and analyzed by a blinded investigator using ImageJ (version 1.49; National Institutes of Health). Five images at magnification ×20 were captured per section from similar topographical regions. Images were decomposed to red-blue-green composites, thresholded using the same upper and lower bounds for all images analyzed, and presented as the mean percent $CD31^+$ area per field of view at magnification ×20. These measurements were interpreted as being proportional to the density of the capillary bed in the muscle. Myofiber cross-sectional areas were quantified by thresholding dystrophin-positive signal until segmentation was achieved and analyzing the area of each complete fiber in the field of view using ImageJ (version 1.49; National Institutes of Health). Myofiber areas were measured in microns squared and presented as a ratio of the treated (ischemic or CTX-injected) to the contralateral control limb. Muscle fiber type IF staining was performed as previously described.[4] Briefly, transverse sections were allowed to come to RT and were fixed/permeabilized with ice-cold 1:1 acetone/methanol for 10 minutes at 4°C. Fixed sections were allowed to air dry for 5 minutes at RT and rehydrated in 1× PBS before blocking in 5% normal goat serum (Sigma-Aldrich) in 1× PBS at RT for 45 minutes. Slides were then incubated overnight at 4°C in a primary antibody solution including antigens directed at dystrophin, MyHC type I, MyHC type IIa, or MyHC type IIb (MyHC type IIx would be unstained). Slides were washed three times in 1× PBS at RT and incubated for 1 hour at RT in the dark in a secondary solution containing a 1:250 dilution of Alexa Fluor secondary antibodies in blocking solution. Sections were washed in the dark three times for 5 minutes each with 1× PBS at RT, and coverslips were mounted using Vectashield HardSet Mounting Medium with DAPI (H-1500; Vector Laboratories). Images were captured using a Life Technologies Evos auto FL wide field fluorescence microscope (Thermo Fisher Scientific) and analyzed by a blinded investigator using ImageJ (version 1.49; National Institutes of Health). Four images at magnification ×10 were captured per section from similar topographical regions using a Life Technologies Evos auto FL wide field fluorescence microscope (Thermo Fisher Scientific) and analyzed by a blinded investigator using ImageJ (version 1.49; National Institutes of Health). Data are presented as the percentage of total myofibers of each fiber type (MyHC type I, MyHC type IIa, or MyHC type IIb).

Immunoblot analysis. EDL muscles were isolated and snap frozen in liquid nitrogen. Frozen muscles were homogenized in ice-cold radioimmunoprecipitation assay buffer (RIPA) Lysis buffer containing protease and phosphatase inhibitors. Protein concentrations were determined using a bicinchoninic acid (BCA) protein assay (Pierce, Thermo Fisher Scientific; #23225). Proteins were then separated using a sodium dodecyl sulfate polyacrylamide gel electrophoresis gel (Mini-Protean TGX; Bio-Rad, Raleigh, NC, #4561093) with 50 μg total protein loaded per well. Blots were visualized with chemiluminescence using standard film procedures.

Preparation of isolated skeletal muscle mitochondria. Skeletal muscle mitochondria were isolated from the plantar flexor (ie, gastrocnemius, plantaris, and soleus) muscles of contralateral control and ischemic hind limbs as previously described.[5] Muscle was pooled from two animals to ensure sufficient mitochondrial yield was obtained. After dissection, muscle was washed in mitochondrial isolation medium (MIM) containing 300 mM sucrose, 10 mM HEPES, and 1 mM EGTA. Muscle was minced on ice using fine-tipped scissors for 5 minutes. Muscle was then washed and resuspended in MIM with 1 mg/mL bovine serum albumin

(BSA) and homogenized on ice using a Teflon pestle and Wheaton overhead stirrer. The homogenate was centrifuged at 800*g* to pellet nonmitochondrial myofibrillar proteins, nuclei, and other cellular components. The supernatant was transferred to a prechilled oakridge tube and then centrifuged at 12,000*g* to pellet mitochondria. The mitochondrial pellet was washed and resuspended in 100 μL of MIM and stored on ice until analysis (<1 hour). Mitochondrial protein content was determined by BCA protein assay (Pierce, Thermo Fisher Scientific).

Mitochondrial respiration measurements. High-resolution O_2 consumption measurements were conducted at 37°C in buffer Z (105 mM K-MES, 30 mM KCl, 1 mM EGTA, 10 mM K_2HPO_4, 5 mM $MgCl_26H_2O$, 0.5 mg/mL BSA, pH 7.1), supplemented with creatine monohydrate (20 mM), using the OROBOROS O2K Oxygraph (Oroboros Instruments Corp). A substrate inhibitor titration protocol was performed as follows: 2 mM malate + 10 mM glutamate (state 2 respiration), followed by the addition of 4 mM ADP to initiate state 3 respiration supported by complex I substrates, convergent electron flow through complexes I and II was initiated with the addition of 10 mM succinate, 10 μM rotenone was subsequently added to inhibit complex I, followed by 10 μM cytochrome C to test the integrity of the mitochondrial membrane, complex IV-supported respiration was examined using the electron donor N,N,N′,N′-tetramethyl-p-phenylenediamine (TMPD) at 0.5 mM in the presence of 2 mM ascorbate (to limit auto-oxidation of TMPD) and 5 μM of antimycin A (to prevent reverse electron flow through complex III), finally, uncoupled respiration was assessed with the addition of 0.5 μM carbonyl cyanide-4-(trifluoromethoxy)phenylhydrazone. The rate of respiration was expressed as pmol/s/mg mitochondrial protein.

Preparation of permeabilized muscle fibers. During sacrifice, a portion of the red gastrocnemius muscle was removed and immediately placed in ice-cold buffer X (50 mM K-MES, 7.23 mM K_2 EGTA, 2.77 mM CaK_2 EGTA, 20 mM imidazole, 20 mM taurine, 5.7 mM adenosine triphosphate, 14.3 mM phosphocreatine, and 6.56 mM $MgCl_2$-$6H_2O$, pH 7.1) for preparation of permeabilized fiber bundles as previously described.[6] Fiber bundles were separated along their longitudinal axis using needle-tipped forceps under magnification (MX6 Stereoscope, Leica Microsystems, Buffalo Grove, Ill), permeabilized with saponin (30 μg/mL) for 30 minutes at 4°C, and then washed in cold buffer Z (105 mM K-MES, 30 mM KCl, 1 mM EGTA, 10 mM K_2HPO_4, 5 mM $MgCl_2$-$6H_2O$, 0.5 mg/mL BSA, pH 7.4) for approximately 20 minutes until analysis. At the conclusion of each experiment, permeabilized fiber bundles were washed in double-distilled H_2O to remove salts, freeze-dried (Labconco, Kansas City, Mo), and weighed. Typical fiber bundle sizes were 0.2-0.4 mg dry weight.

Isolated myofiber respiration measurements. High-resolution O_2 consumption measurements were conducted at 37°C in buffer Z (105 mM K-MES, 30 mM KCl, 1 mM EGTA, 10 mM K_2HPO_4, 5 mM $MgCl_26H_2O$, 0.5 mg/mL BSA, pH 7.1), supplemented with creatine monohydrate (20 mM), using the OROBOROS O2K Oxygraph (Oroboros Instruments Corp). An abbreviated protocol similar to that used for isolated mitochondria was performed, described as follows: 2 mM malate with 10 mM glutamate (state 2 respiration), followed by the addition of 4 mM ADP to initiate state 3 respiration supported by complex I substrates, convergent electron flow was next initiated with the addition of 10 mM succinate, 10 μM rotenone was subsequently added to inhibit complex I, followed by 10 μM cytochrome C to test the integrity of the mitochondrial membrane. The rate of respiration was normalized to the myofiber dry weight and expressed as pmol/s/mg dry weight.

Mitochondrial calcium retention capacity. To determine susceptibility to opening of the mitochondrial permeability transition pore, preparations of isolated mitochondria were exposed to progressively increasing calcium load in the presence of (in mM): 5 malate, 10 glutamate, 0.02 ADP. Changes in extramitochondrial calcium concentration were monitored fluorometrically using Calcium Green (1 μM, excitation/emission 506/532 nm, Invitrogen) per the manufacturer's instructions. All experiments were run at 37°C in Buffer Z containing 2 U/mL hexokinase and 5 mM 2-deoxyglucose (to clamp respiration).

Citrate synthase activity assays. Activity assays were performed using a citrate synthase activity assay kit (Sigma-Aldrich). Briefly, EDL muscles were isolated and snap frozen in liquid nitrogen. Frozen muscles were homogenized in ice-cold Lysis buffer. Protein concentrations were determined using a BCA protein assay (Pierce, Thermo Fisher Scientific; #23225). Activity assays were performed in assay buffer containing (in mM): 100 Tris, 1 EDTA, 1 EGTA, 10 DTNB (Sigma-Aldrich: D8130), and 30 Acetyl CoA at pH 8.35. All samples were measured in triplicate and the average absorbance was used in final calculations of activity. Background absorbance was measured before addition of 10 mM oxoloacetate (Sigma-Aldrich: 04126) and final activity rates were corrected for those values.

Muscle contractile force measurements. Contractile force was performed as previously described.[7] In brief, single EDL muscles were surgically excised with ligatures at each tendon (5-0 silk suture) and mounted in a bath between a fixed post and force transducer (300B-LR; Aurora Scientific, Aurora, ON, Canada) operated in isometric mode. The muscle was maintained in modified Kreb buffer solution (pH 7.2) containing (in mM) 115 NaCl, 2.5 KCl, 1.8 $CaCl_2$, 2.15 Na_2HPO_4, 0.85 NaH_2PO_4, and maintained at 25°C under aeration with 95% O_2/5% CO_2 throughout the experiment. Resting tension and muscle length were iteratively adjusted for each muscle to obtain the optimal twitch force and a supramaximal stimulation current of 600 mA was used for stimulation. After a 5-minute equilibration, isometric tension was evaluated by 200-ms trains of pulses delivered at 10, 20, 40, 60, 80, 100, and 120 Hz. Length was determined with a digital microcaliper. After the experimental protocol, muscles

were trimmed proximal to the suture connections, excess moisture was removed, and the muscle was weighed. The cross-sectional area for each muscle was determined by dividing the mass of the muscle (g) by the product of its length (L_0, mm) and the density of muscle (1.06 g/cm^3) and was expressed as millimeters squared. Muscle output was then expressed as specific force (N/cm^2) determined by dividing the tension (N) by the muscle cross-sectional area.

Total RNA and qRT-PCR gene expression. Total RNA was extracted from mouse EDL muscles using TRIzol (Invitrogen) phenol/chloroform extraction. RNA was reverse-transcribed using SuperScript IV Reverse Transcriptase and random primers (Invitrogen). Reactions were incubated at 50°C for 50 minutes and at 85°C for 5 minutes. Real-time polymerase chain reaction was performed using an ABI ViiA-7 system (Applied Biosystems). Relative quantification of MyoD family inhibitor, muscle atrophy F-box, muscle ring finger protein-1, TNFα, IL-1 β, and IL-6 mRNA levels were determined using the comparative cycles to threshold (ΔΔCT) method using FAM TaqMan gene expression assays (Thermo Fisher Scientific) specific for each of these genes run in complex (multiplex) with a VIC-labeled 18-S ribosomal subunit control primer.

Statistics. Data are presented as a ratio of the treated (ischemic or CTX-injected) left (L) to the untreated (nonischemic or saline injected) right (R) limb and mean ± standard error of the mean. Force frequency and fiber typing data are presented as L and R for each strain, mean ± standard error of the mean. Statistical analyses were carried out using StatPlus:mac (version 2009; AnalystSoft), Vassarstats (www.vassarstats.net), or Prism 6 (version 6.0d; Graphpad Software Inc) software. Two sided *t*-tests were performed a priori to examine mean differences in the control limbs of the strains. All other data were compared using analysis of variance with Holm-Sidak multiple comparison test or uncorrected Student two-tailed *t*-test. In all cases, $P < .05$ was considered statistically significant.

SUPPLEMENTAL REFERENCES

1. McClung JM, McCord TJ, Southerland K, Schmidt CA, Padgett ME, Ryan TE, et al. Subacute limb ischemia induces skeletal muscle injury in genetically susceptible mice independent of vascular density [published online ahead of print August 5, 2015]. J Vasc Surg doi: 10.1016/j.jvs.2015.06.139.
2. Yan Z, Choi S, Liu X, Zhang M, Schageman JJ, Lee SY, et al. Highly coordinated gene regulation in mouse skeletal muscle regeneration. J Biol Chem 2003;278:8826-36.
3. McClung JM, McCord TJ, Keum S, Johnson S, Annex BH, Marchuk DA, et al. Skeletal muscle-specific genetic determinants contribute to the differential strain-dependent effects of hindlimb ischemia in mice. Am J Pathol 2012;180:2156-69.
4. McClung JM, Van Gammeren D, Whidden MA, Falk DJ, Kavazis AN, Hudson MB, et al. Apocynin attenuates diaphragm oxidative stress and protease activation during prolonged mechanical ventilation. Crit Care Med 2009;37:1373-9.
5. Lark DS, Reese LR, Ryan TE, Torres MJ, Smith CD, Lin CT, et al. Protein kinase A governs oxidative phosphorylation kinetics and oxidant emitting potential at complex I. Front Physiol 2015;6:332.
6. Perry CG, Kane DA, Lin CT, Kozy R, Cathey BL, Lark DS, et al. Inhibiting myosin-ATPase reveals a dynamic range of mitochondrial respiratory control in skeletal muscle. Biochem J 2011;437:215-22.
7. Spangenburg EE, Le Roith D, Ward CW, Bodine SC. A functional insulin-like growth factor receptor is not necessary for load-induced skeletal muscle hypertrophy. J Physiol 2008;586:283-91.

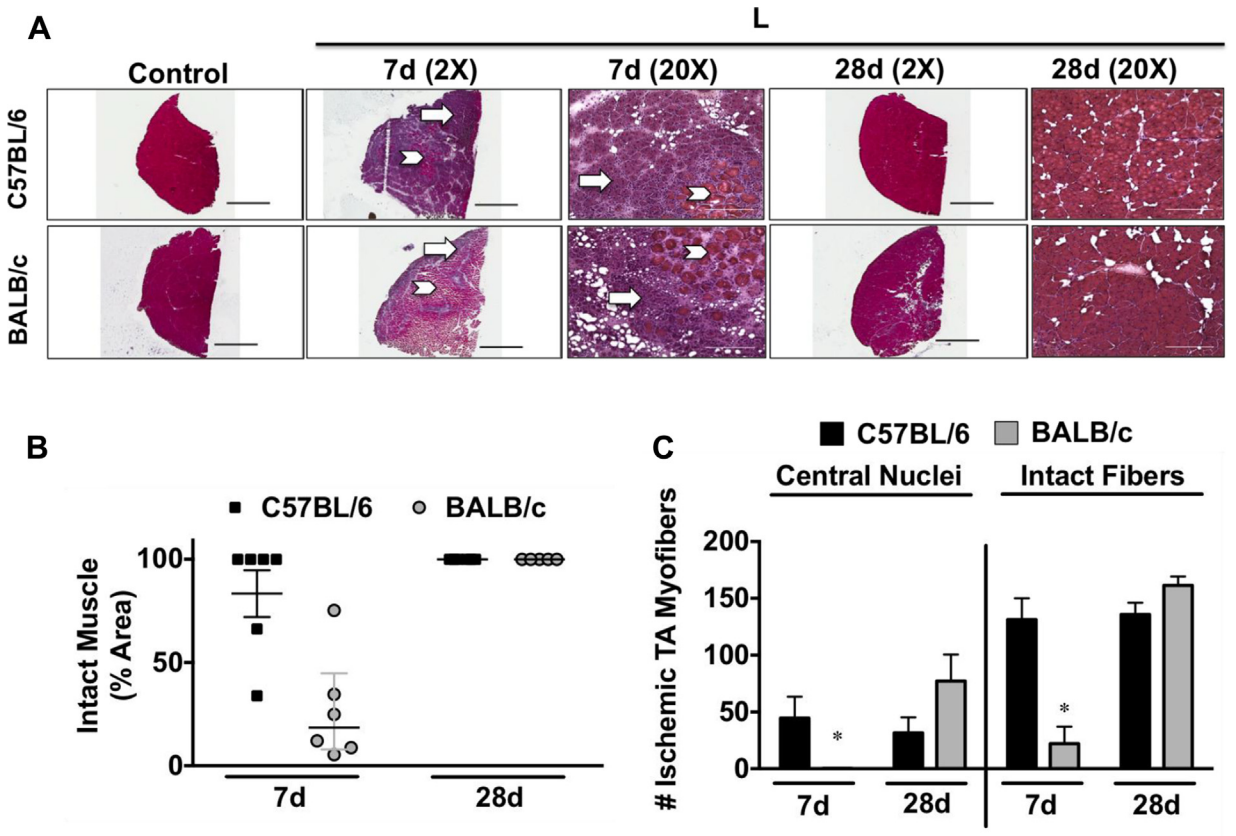

Supplementary Fig 1 (online only). Strain dependent myopathy with subacute hind limb ischemia (SLI). Subacute femoral artery occlusion was performed on C57BL/6 and BALB/c mice by placement of a single ameroid constrictor on the proximal portion of the femoral artery, immediately proximal to the epigastric arterial branch. **A,** The *scale bar* inlays are 1000 μm in length (2X), and 200 μm in length (20X). Representative 2X and 20X images of hematoxylin and eosin (H&E) stained sections of tibialis anterior (*TA*) muscles subjected to 7 and 28 days of subacute ischemia. The *arrows* indicate intact muscle; *chevrons* indicate regions of anucleate necrotic fibers. **B,** Muscle regeneration was quantified from 2X H&E images by measuring the total regions of interest (*Area*) containing necrotic/anuclueate myofibers and subtracting from total muscle area to give a percent area of intact muscle, which is represented by median and interquartile range. **C,** Total myofibers with centralized nuclei (*Central Nuclei*) and total myofiber number (*Intact Fibers*) were determined in representative images at magnification ×10. Data are represented as mean ± standard error of the mean. All data are representative of n = 6 per strain per time point for each observation. $^{*}P < .05$ vs day matched C57BL/6. *d*, Days; *L*, ischemic limb; *R*, nonischemic contralateral control limb.

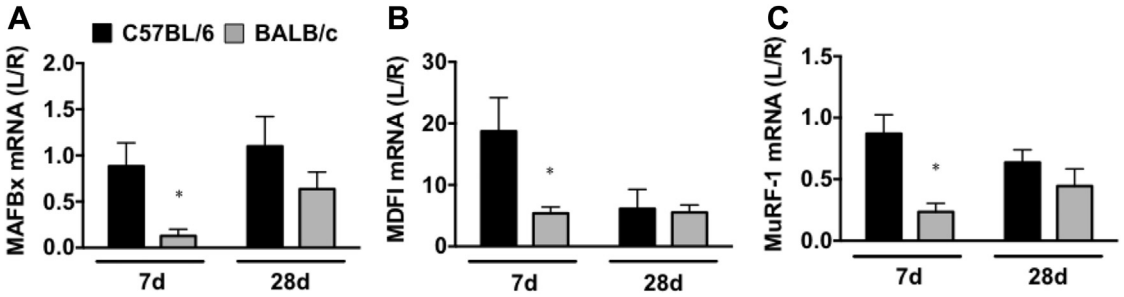

Supplementary Fig 2 (online only). Atrophy-associated gene expression in ischemic hind limbs. Subacute femoral artery occlusion was performed on C57BL/6 and BALB/c mice by placement of a single ameroid constrictor on the proximal portion of the femoral artery. Quantitative reverse transcription-polymerase chain reaction (qRT-PCR) was used to determine extensor digitorum longus (EDL) messenger RNA (mRNA) expression of **(A)** muscle atrophy F-box (*MAFBx*), **(B)** MyoD family inhibitor 1 (MDFI), and **(C)** muscle ring finger protein-1 (*MuRF-1*). Data are representative of corrected values for ribosomal subunit 18S mRNA and expressed as a ratio of the ischemic (*L*) to the nonischemic contralateral control (*R*) limb; mean ± standard error of the mean. n = 6 per strain per time point for each observation. $^{*}P < .05$ vs day matched C57BL/6. *d*, Days.

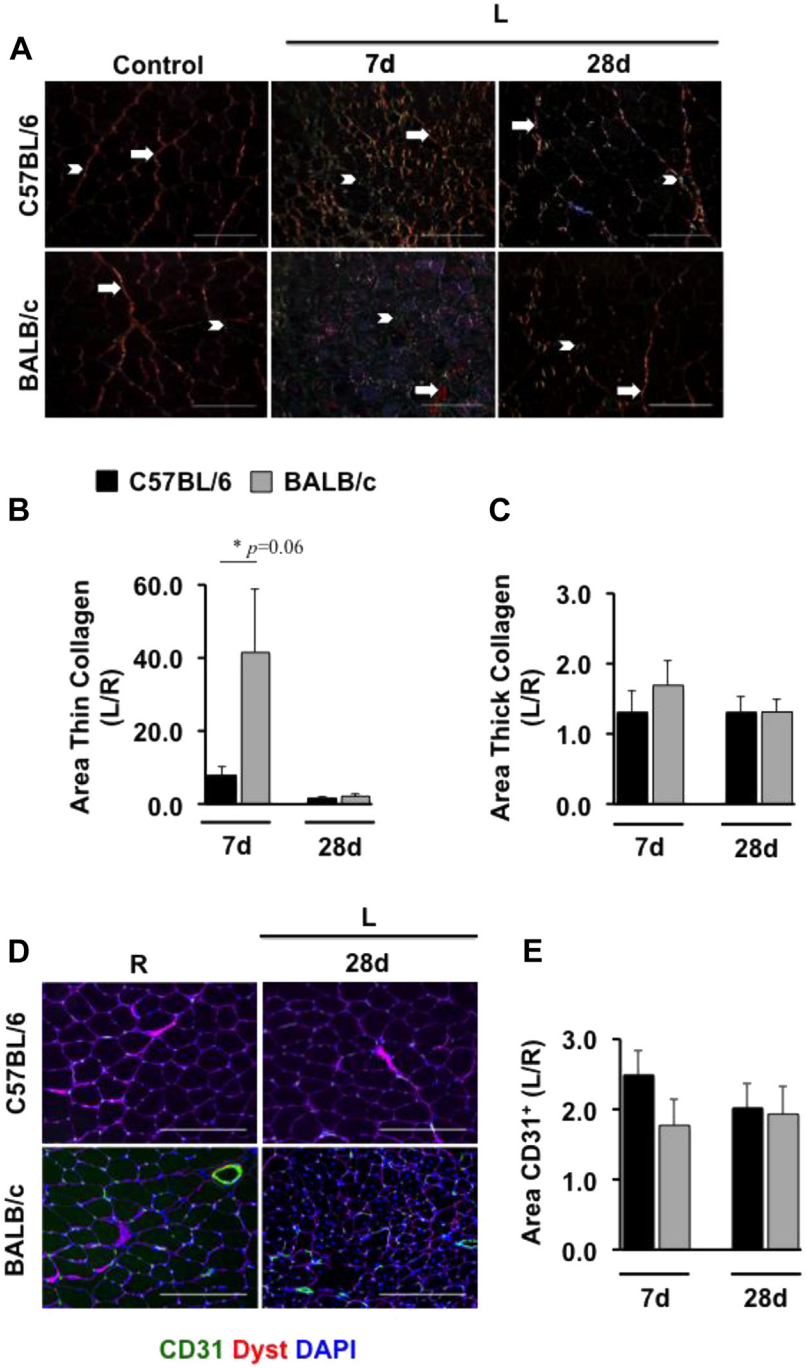

Supplementary Fig 3 (online only). Nonmyofiber tissue deposition in ischemic hind limb muscle. Subacute femoral artery occlusion was performed on C57BL/6 and BALB/c mice by placement of a single ameroid constrictor on the proximal portion of the femoral artery. **A,** Sections of tibialis anterior (TA) muscles were stained with picrosirius red (PR) dye (birefringent dye) to determine collagen deposition. Representative images at magnification ×10 of PR dye taken through a polarized light filter at 7 and 28 postoperative days (*d*). The *arrows* indicate regions containing thick collagen (*orange/red* birefringence); *chevrons* indicate regions containing thin collagen (*green/yellow* birefringence). The *scale bar* inlays are 400 μm in length. **B,** *Green/yellow* hue distribution (thin collagen deposition). **C,** *Orange/red* hue distribution (thick collagen deposition). **D,** Sections of TA muscles were immunofluorescently stained for CD31 ($CD31^+$; PECAM-1^+) for the analysis of capillary density (**E**). The *scale bar* inlays are 200 μm in length. All data are presented as the ratio of the ischemic (*L*) to the nonischemic contralateral control (*R*) limb, mean ± standard error of the mean and representative of n ≥ 6 per strain per time point. $^*P = .06$ vs day matched C57BL/6. *DAPI,* 4′,6-diamidino-2-phenylindole; *Dyst,* dystrophin.

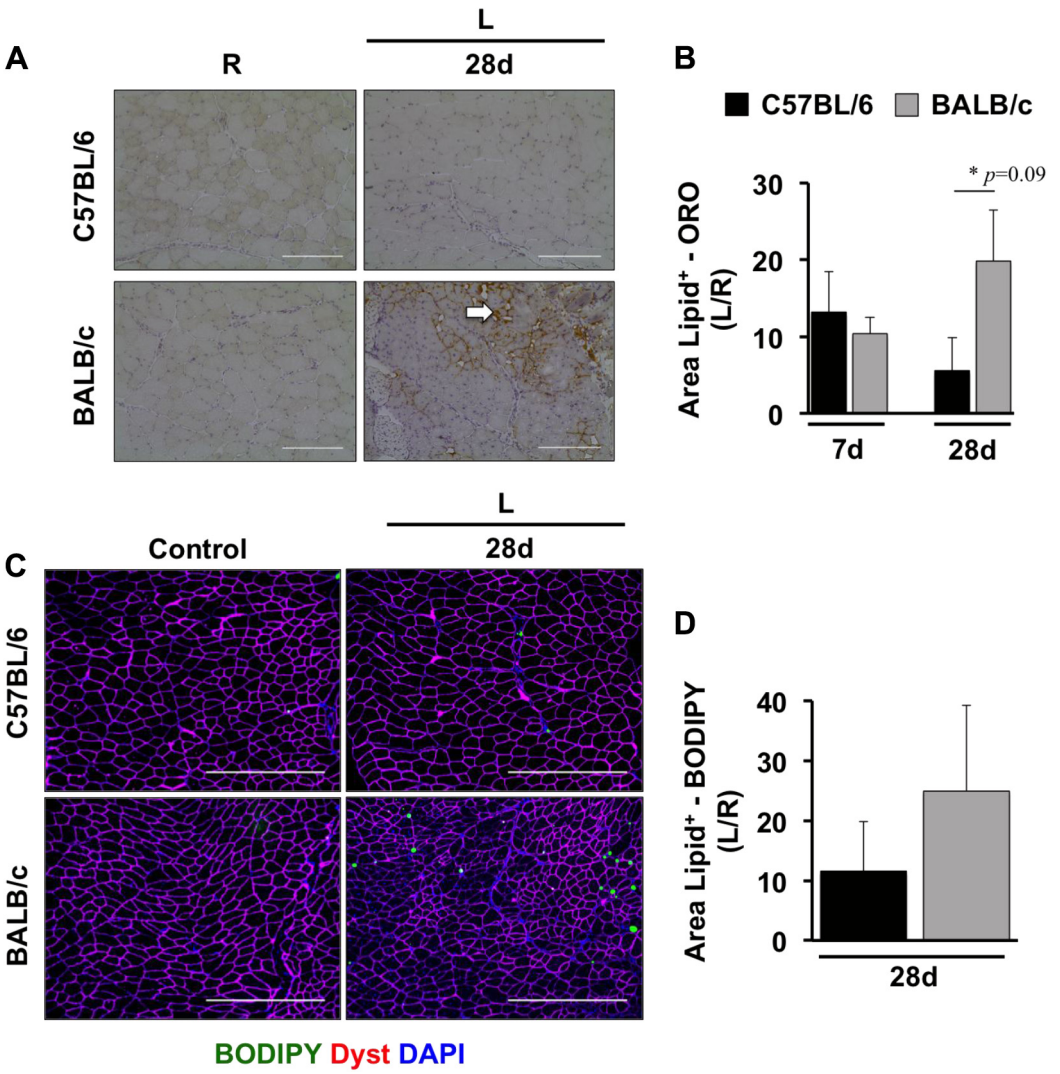

Supplementary Fig 4 (online only). Strain dependent intramuscular lipid content during ischemia. Subacute femoral artery occlusion was performed on C57BL/6 and BALB/c mice by placement of a single ameroid constrictor on the proximal portion of the femoral artery. **A,** Sections of tibialis anterior (TA) muscle were histologically stained with Oil Red-O (*ORO*) to determine muscle lipid content. *Scale bar* inlays are 400 μm in length. The *arrow* indicates region of lipid-positive staining **(B)**. **C,** Sections of TA muscles were also fluorescently labeled with boron dipyrromethene (*BODIPY*) for the determination of intermuscular lipid inclusions. *Scale bar* inlays are 400 μm in length. **D,** All data are presented as ratio of the ischemic (*L*) to the nonischemic contralateral control (*R*) limb; mean ± standard error of the mean and representative of n = 6 per strain per time point for each observation. Nonsignificant trend observed at 28 days (*d*) for ORO ($P = .09$). *DAPI,* 4′,6-diamidino-2-phenylindole; *Dyst,* dystrophin.

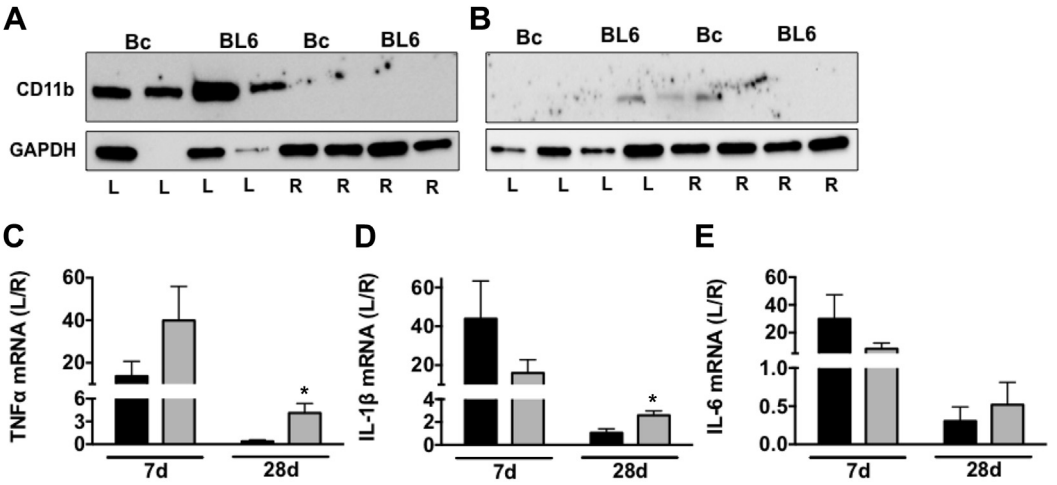

Supplementary Fig 5 (online only). Skeletal muscle innate immune response during ischemia. Subacute femoral artery occlusion was performed on C57BL/6 (*BL6*) and BALB/c (*Bc*) mice by placement of a single ameroid constrictor on the proximal portion of the femoral artery. Western blot analysis was performed for qualitative observation of macrophage-1 antigen (Mac-1; *CD11b*) protein abundances, with glyceraldehyde 3-phosphate dehydrogenase (*GAPDH*) protein blotting as a loading reference **(A)** and **(B)**. Quantitative reverse transcription-polymerase chain reaction (qRT-PCR) was used to determine extensor digitorum longus (EDL) messenger RNA (*mRNA*) expression of tumor necrosis factor α (*TNFα*; **C**), interleukin (*IL*)-1β **(D)**, and IL-6 **(E)**. Data are representative of corrected values for ribosomal 18S subunit mRNA and expressed as a ratio of the ischemic (*L*) to the nonischemic contralateral control (*R*) limb; mean ± standard error of the mean. n = 6 per strain per time point for each observation. $^{*}P < .05$ vs day matched C57BL/6. *d,* Days.

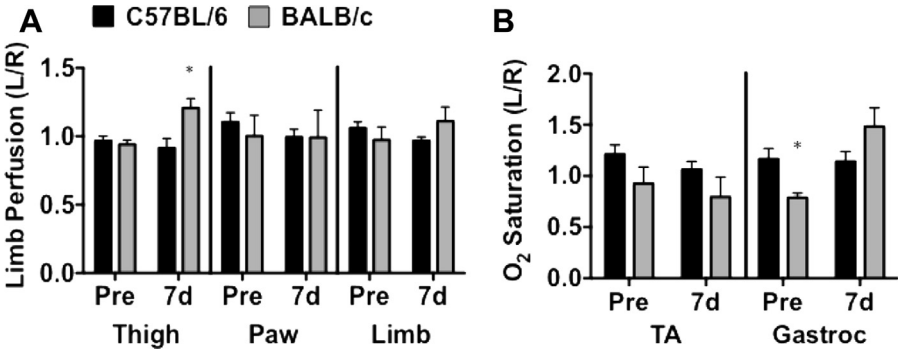

Supplementary Fig 6 (online only). Verification of myotoxin injury as nonischemic. Cardiotoxin was injected intramuscularly into the tibialis anterior (*TA*) and the lateral/medial heads of the gastrocnemius (*Gastroc*) muscle. A sham injection of equal volume sterile saline was injected in the same muscles in the contralateral control limb (*R*). **(A)** Laser Doppler perfusion imaging (LDPI) was performed and regionally analyzed (thigh, paw, and whole limb). **(B)** Tissue O_2 saturation was measured via white light reflectance spectroscopy over the TA and Gastroc muscles after injury. Data are representative of the ratio of the CTX-injected (*L*) to the contralateral control (*R*) limb; mean ± standard error of the mean. All data are representative of n = 6 per strain per time point for each observation. $^{*}P < .05$ vs day matched C57BL/6. *d,* Days; *Pre,* baseline.

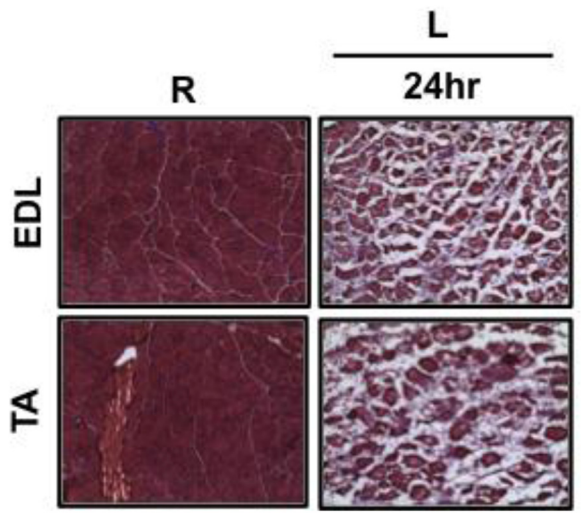

Supplementary Fig 7 (online only). Distribution of myotoxic injury to the anterior limb compartment. Cardiotoxin (CTX) was injected intramuscularly into the tibialis anterior (*TA*) and the lateral/medial heads of the gastrocnemius muscle. Representative images at magnification ×20 of hematoxylin and eosin (H&E) stained sections of TA and extensor digitorum longus (*EDL*) muscles 24 hours (*24 hr*) after CTX injection into the TA. *L*, CTX-injected limb; *R*, contralateral control limb.

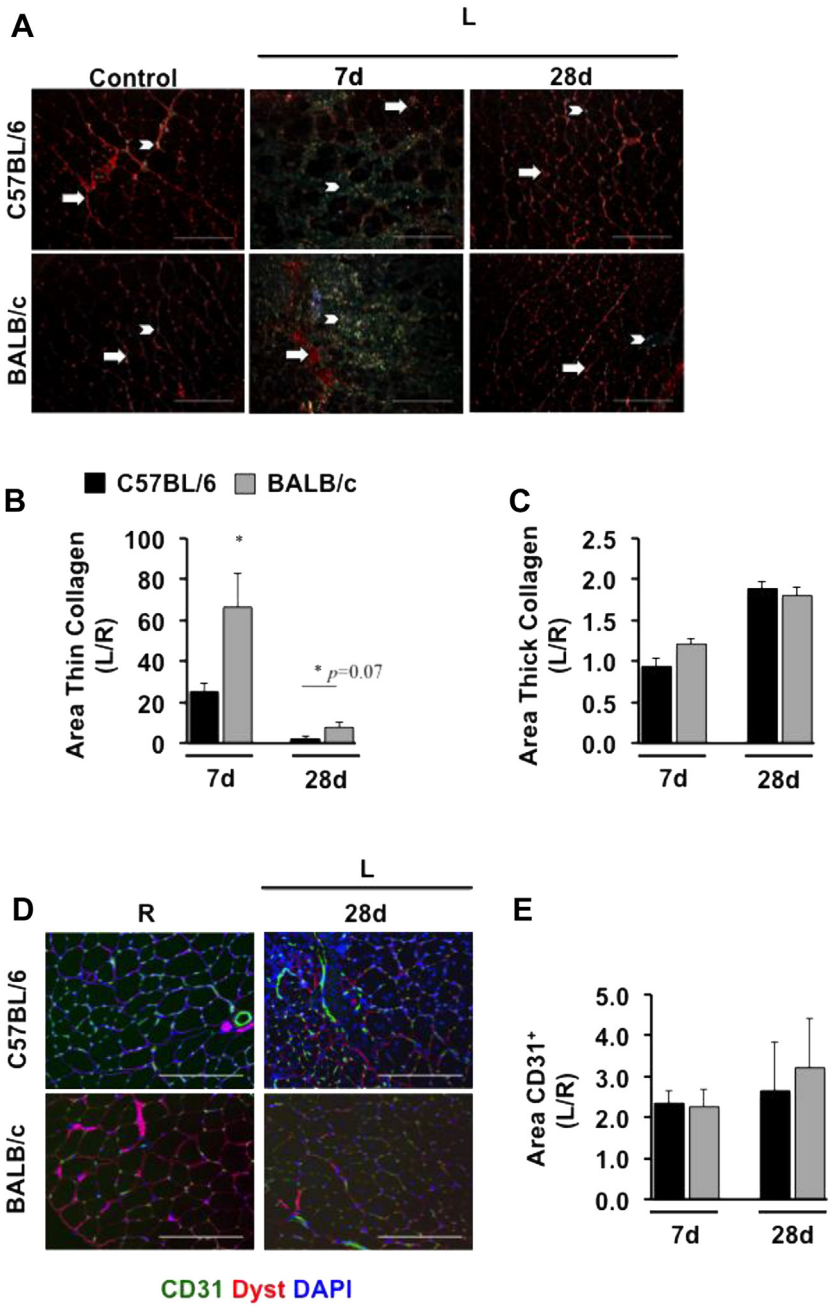

Supplementary Fig 8 (online only). Nonmyofiber tissue deposition in nonischemic regenerating muscle. Nonischemic muscle regeneration was induced by cardiotoxin injection. **A,** Sections of tibialis anterior (TA) muscles were stained with picrosirius red (PR) (birefringent dye) to determine collagen deposition. Representative images at magnification ×10 of PR dye taken through a polarized light filter at 7 and 28 postoperative days (*d*). The *arrows* indicate regions containing thick collagen (*orange/red* birefringence); *chevrons* indicate regions containing thin collagen (*green/yellow* birefringence). The *scale bar* inlays are 400 μm in length. **B,** *Green/yellow* hue distribution (thin collagen deposition). **C,** *Orange/red* hue distribution (thick collagen deposition). **D,** Sections of TA muscle were immunofluorescently labeled with CD31-positive ($CD31^+$; *CD31*; PECAM-1^+) for the analysis of capillary density **(E)**. The *scale bar* inlays are 200 μm in length. All data are presented as ratio of the CTX-injected (*L*) to the contralateral control (*R*) limb; mean ± standard error of the mean and representative of n ≥ 6 per strain per time point. $^*P < .05$ vs day matched C57BL/6, or indicated nonsignificant trend vs day matched C57BL/6 thin collagen ($P = .07$). *DAPI,* 4′,6-diamidino-2-phenylindole (DAPI); *Dyst,* dystrophin.

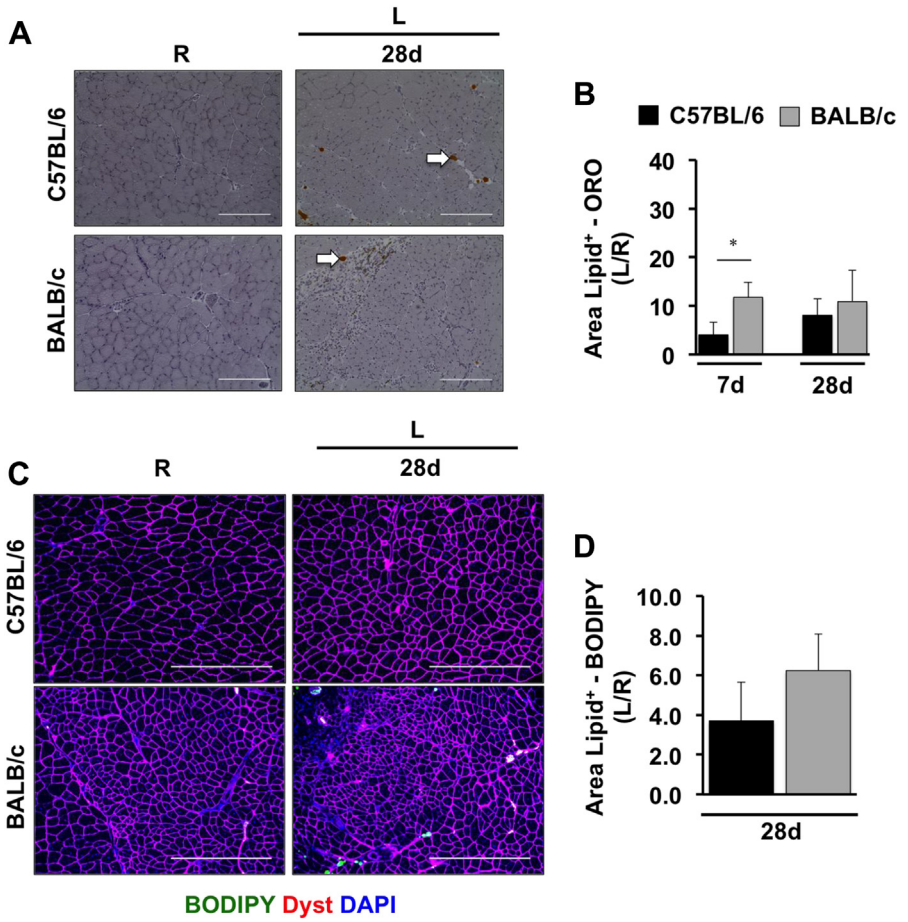

Supplementary Fig 9 (online only). Strain dependent intramuscular lipid content during nonischemic injury. Cardiotoxin was injected intramuscularly into the tibialis anterior (TA) and the lateral/medial heads of the gastrocnemius muscle. **A,** Sections of TA muscle were stained with Oil Red-O (*ORO*) to determine muscle lipid content. The *scale bar* inlays are 400 μm in length. The *arrows* indicate regions of lipid positive staining **(B)**. **C,** Sections of TA muscles were also fluorescently labeled with boron dipyrromethene (*BODIPY*) for the determination of intermuscular lipid inclusions. The *scale bar* inlays are 400 μm in length **(D)**. All data are presented as ratio of the CTX-injected (*L*) to the contralateral control limb (*R*) limb; mean ± standard error of the mean and representative of n = 6 per strain per time point for each observation. * Nonsignificant trend observed at 7 days (*d*) for ORO ($P = .07$). *Dyst*, dystrophin.